Oxidation Resistant, Cr Retaining, Electrically Conductive Coatings on Metallic Alloys for SOFC Interconnects

Final Report

Reporting Period Start Date 9/15/04

Reporting Period End Date 03/31/08*
*Phase I End Date 3/14/06
(re-submitted after NETL review)

Principal Author:
Vladimir I. Gorokhovsky, PhD

December 2, 2008

DOE Award Number: DE-FC26-04NT42225

Arcomac Surface Engineering, LLC
151 Evergreen, Suite D
Bozeman, MT 59715

ABSTRACT:

This report describes significant results from an on-going, collaborative effort to enable the use of inexpensive metallic alloys as interconnects in planar solid oxide fuel cells (SOFCs) through the use of advanced coating technologies. Arcomac Surface Engineering, LLC, under the leadership of Dr. Vladimir Gorokhovsky, is investigating filtered-arc and filtered-arc plasma-assisted hybrid coating deposition technologies to promote oxidation resistance, eliminate Cr volatility, and stabilize the electrical conductivity of both standard and specialty steel alloys of interest for SOFC metallic interconnect (IC) applications. Arcomac has successfully developed technologies and processes to deposit coatings with excellent adhesion, which have demonstrated a substantial increase in high temperature oxidation resistance, stabilization of low Area Specific Resistance values and significantly decrease Cr volatility. An extensive matrix of deposition processes, coating compositions and architectures was evaluated. Technical performance of coated and uncoated sample coupons during exposures to SOFC interconnect-relevant conditions is discussed, and promising future directions are considered. Cost analyses have been prepared based on assessment of plasma processing parameters, which demonstrate the feasibility of the proposed surface engineering process for SOFC metallic IC applications.

TABLE OF CONTENTS:

EXECUTIVE SUMMARY:

Reduced operating temperatures (600-800°C) of Solid Oxide Fuel Cells (SOFCs) may enable the use of inexpensive ferritic steels as interconnects. Due to the demanding SOFC interconnect operating environment, protective coatings are gaining attention to increase long-term stability. Arcomac Surface Engineering, LLC (ASE), under the leadership of Dr. Vladimir Gorokhovsky, is investigating filtered-arc and filtered-arc plasma-assisted hybrid coating deposition technologies to promote oxidation resistance, eliminate Cr volatility and stabilize the electrical conductivity of both standard and specialty steel alloys of interest for SOFC interconnects. Arcomac has successfully developed technologies, equipment, and processes to deposit coatings with excellent adhesion, which have demonstrated a substantial increase in high temperature oxidation resistance, stabilization of low area specific resistance (ASR) values and significantly decreased Cr volatility. Evaluation of deposition processes, coating compositions and architectures is now continuing with Industrial SOFC developers.

The unique flexibility of Arcomac's vapor deposition technologies permits controlled deposition of a wide variety of coating compositions and architectures, with attributes often unattainable using conventional coating approaches. Arcomac's Filtered arc Plasma Source Ion Deposition (FAPSID) surface engineering process utilizes filtered cathodic arc, unbalanced magnetron (UBM), electron beam physical vapor deposition (EB-PVD) and thermal resistive evaporation physical vapor deposition (TRE-PVD) sources in one universal coating system layout. This capability allows plasma vapor deposition from a large selection of coating material, and allows unique coating architectures to be created in one vacuum cycle. In Phase I of this project, large area filtered arc deposition (LAFAD) and hybrid filtered arc deposition assisted electron beam physical vapor deposition (FAD/EBPVD) technologies were used to deposit two-segment coatings with Cr-Co-Al-O-N based nanolaminated cermet bottom segments and Mn-Co-O spinel top segments. The bottom segment serves as a diffusion barrier against oxygen inward diffusion and as an adhesion promoting bond segment, yet provides high electronic conductivity at 800ºC. The top segment is intended to inhibit Cr volatility and provide improved cathode contact compatibility, while also having high electrical conductivity at 800ºC. Coatings were deposited on ferritic steel coupons (Crofer 22APU, 441 and 430 stainless steels) and subsequently annealed in air for various time intervals. Surface oxidation and high temperature thermal-chemical stability were investigated using RBS, XRD, and both surface and cross sectional SEM/EDS analyses. Cr-volatilization was evaluated using a transpiration apparatus and ICP-MS analysis of the resultant condensate. Electrical conductivity (ASR) was studied as a function of time using the four-point probe technique. The oxidation behavior, Cr volatilization rate, and electrical conductivity of the coated samples were observed to be highly favorable compared with the uncoated samples. Phase II expanded upon Phase I efforts by combining the two-layer coating system into a multi-elemental nanocomposite coating with varying amounts of Co, Mn, Al, Cr, Ti, and Y. Several of these coatings exhibited excellent SOFC(IC)-relevant performance on ferritic stainless steels in simulated environments. SOFC stack testing at Versa Power Systems (VPS) is currently being conducted for VPS interconnects with optimized coatings.

The two phase SECA Core Technology project allowed Arcomac to evaluate a myriad of deposition processes and coatings for their efficacy in planar SOFC interconnect applications. Promising candidates for coating compositions and architectures were identified, and deposition processes were found amenable to high-volume manufacturing. Arcomac is continuing to

develop promising coating material systems and is currently working with commercial SOFC system developers.

REPORT DETAILS

Phase I work

Experimental methods:

Coating architectures and plasma vapor deposition processes

A broad goal of this research is to enable the use of inexpensive alloys for SOFC interconnects by developing a coating material system and deposition process to ensure electrical, chemical and thermal-mechanical compatibility with other SOFC stack components, throughout the device's life-time. Toward this end, the dual segment coating approach, illustrated in Figure 1, has been investigated.

The use of coatings to improve oxidation resistance on metal alloys has been known for many years. The LAFAD Co-Cr-Al-Y-O-N bottom-segment coating system was selected for this study due to previously demonstrated oxidation and wear resistance at temperatures up to 900°C [2,11-13,24,25]. Nanolayered structures consisting of alternating Al(O/N) and Cr/Co(O/N) layers have been investigated with the goal of revealing the application-specific efficacy of this surface treatment (the notation "O/N" is meant to denote all oxygen and nitrogen-containing species generally). In addition, both pure nitrides and oxides have been explored through this work.

The hybrid LAFAD+EBPVD $Mn_{1.5}Co_{1.5}O_4$ spinel system was investigated as a top segment coating because of its SOFC cathode compatibility, its recently reported success in reducing ASR, as well as its anticipated reduction in Cr volatilization [14-16,27].

Two primary coating architectures were investigated during Phase I of the project: one with the top $Mn_{1.5}Co_{1.5}O_4$ segment only (~2μm); and, one with both the sublayer Cr/Co/Al(O/N) bond coating segment and top segment present (~4μm). Results from long-term (>2000hrs) oxidation in air at 800°C, ASR and Cr volatility from the two unique coated samples, in addition to uncoated samples are presented here, together with an interpretation of the significance of these results.

The single and dual segment coatings were deposited on ~1.6cm^2 x 1mm thick mechanically-lapped and polished (50-80nm nominal roughness by LapRite, Inc) substrate coupons of both commercial 430 stainless steel and Crofer 22 APU by Arcomac Surface Engineering, LLC using a patented Filtered Arc Plasma Source Ion Deposition (FAPSID) technology [7,27,29]. FAPSID employs a rectangular plasma-guide chamber with two rectangular deflecting coils installed on opposite sides, with electron beam evaporators within the chamber, as shown in Figure 2. In this design, two primary cathodic arc sources utilizing Cr/Co(6%) and Al(99.9%) targets are placed opposite each other on the sidewalls of the plasma-guide chamber, surrounded by rectangular deflecting coils, and separated by an anodic baffle. The FAD vapor plasma source uses a superimposed deflecting magnetic field to turn the metal-ion flow 90° toward the deposition chamber and substrates. The more massive droplets of target material follow straighter trajectories and are captured on baffles, resulting in droplet-free coatings. A set of scanning magnetic coils allows the ion plasma jet to be rastered, thereby promoting uniform coverage of large surface areas [7,17]. When the deflecting magnetic field

coils are off, the LAFAD source can be employed as an effective, large area gaseous plasma generator, which ionizes the vapors from other conventional sources within the chamber. During the EBPVD deposition of the $Mn_{1.5}Co_{1.5}O_4$ upper segment, the LAFAD source is used as a powerful emitter of electrons, effectively ionizing the $Mn_{1.5}Co_{1.5}O_4$ vapor, in an attempt to densify the resultant coating. In this gaseous plasma mode, the deflecting magnetic subsystem of the filtered arc source is deactivated and the cathodes of the primary arc source serve as electron emitters while the distant auxiliary anode accepts the electron current. Ionization rate in the auxiliary arc plasma discharge reaches up to 50%. The metal vapor flow from the e-beam evaporator is also substantially ionized via collisions with the auxiliary arc electrons.

The substrates were mounted on pedestals distributed about the outer rim of a rotating carousel in the FAPSID chamber. Substrate temperature during deposition was about 500°C. Substrates were first cleaned in an Ar ion plasma at $8x10^{-2}$ Pa for 20 min, followed by 2 min of high voltage Cr/Co ion etching in Ar ($2x10^{-2}$ Pa). Cr/Co and Al ions were then deposited in an oxygen/nitrogen/Ar = 1/1/1 atmosphere at ~$4x10^{-2}$ Pa with a squarewave/chopped applied substrate bias voltage of -300V peak at 40 kHz. With both target sources on, and substrate rotation engaged, the substrates were successively exposed alternately to Cr/Co then Al ions, in an atmosphere of both oxygen and nitrogen, resulting in bi-layers of CrCo(O/N)/AlO(N). Thickness of the individual bi-layers, the number of bilayers per total coating segment and the ratio of the sublayers (e.g. CoCrON/AlON) inside of the bilayer period in the coating was controlled by the rotation speed of the carousel, deposition rates and the total coating deposition time. It was estimated at ~2.1 nm for the coatings considered here. The LAFAD/EBPVD $Mn_{1.5}Co_{1.5}O_4$ upper segment coating was deposited by evaporating a sintered $Mn_{1.5}Co_{1.5}O_4$ spinel target pellet using a standard 6kW electron beam rastered over the target, with an emission current ranging from 0.1 to ~0.6A. The pressure during the evaporation was ~$4x10^{-2}$Pa in an atmosphere of oxygen/argon = 1/1. During the evaporation, the LAFAD system was set for ionization mode (deflecting magnetic field off), with an auxiliary arc current of ~100A. The substrate bias during this deposition was set at -60V.

Another FAPSID process that was investigated during Phase I consisted of filtered arc deposition assisted resistive evaporation (LAFAD/RE). In this embodiment, MnO_2 powder was evaporated from an alumina-coated tungsten evaporation boat, while being mixed with filtered arc metal plasma from CrCo and Al targets installed in the LAFAD source. This exemplifies the combinations of vapor plasma sources which can be used to achieve the desired coating composition, architecture and productivity with the FAPSID surface engineering system.

Coating properties characterization

Coating adhesion was assessed by means of the Mercedes indentation test using a Rockwell C indenter with ~100N load. Radial cracks surrounding the indentation indicate good coating adhesion. Radial cracks with localized delamination indicate fair adhesion, and concentric cracks around the indentation with large area delamination indicate poor coating adhesion [18].

Oxidation of the sample coupons (in Bozeman, MT air) was carried out using a standard furnace operated with no control of humidity or air circulation. Measurements of Area Specific Resistance (ASR) were made using standard procedures with Ag paste electrodes [4] on pre-oxidized samples as a function of time and temperature for coated and uncoated Crofer 22 APU coupons. A schematic describing the ASR sample measurement apparatus is shown in Figure 3.

Prior to ASR measurements at MSU, all coupons were oxidized in air at 800°C for 100 hours, with a furnace temperature ramp rate of 5°C/min, to minimize TGO scale spallation. Subsequent to coupon pre-oxidation, Ag paste was applied to a ~1cm^2 contact area on two identical samples and cured for ~30 minutes at 110°C in air (ASR testing at PNNL did not involve pre-oxidation). Two Pt wires were spot welded (local oxide scale/coating removed) to the alloys opposite the Ag paste contact area and the sample sandwich was assembled. To ensure sandwich electrical contact, the assembly was placed between two metal blocks (~0.5kg) with alumina spacers. In addition, one identical 'witness' sample (for subsequent surface analyses) was placed next to the sandwich. The entire apparatus was then inserted into a bench-top furnace with a type-K thermocouple near the apparatus and alumina tubes to insulate the Pt wires.

The following sequence of experimental procedures was used: First, the system is heated to 800°C before applying a small and increasing DC voltage across the sandwich with the electrical current recorded; when the current density reaches ~0.5A/cm^2, the power supply is set to constant current mode and ASR recorded. ASR measurements for coated samples extended to >2400 hours.

Subsequent to varying exposure times, sample cross sections for microscopic analysis were prepared by epoxy mounting, sectioning and polishing. SEM/EDS analysis was performed using a Joel SEM model S4700.

Ion beam analysis of the coated samples was performed using the 3 MV tandem accelerator at the Environmental Molecular Sciences Laboratory (EMSL) at Pacific Northwest National Laboratory (PNNL) in Richland, WA, and the 2 MV van de Graaff accelerator at Montana State University. The latter was used for beams of He+ and H+ up to 2 MeV, while the former provided higher energy He+ beams to analyze thicker coatings, and d+ beams for nuclear reaction analysis of the O and N concentrations, using the $^{14}N(d,p)^{15}N$ and $^{16}O(d,p)^{17}O$ reactions. Spectra were typically collected after total oxidation periods of 1, 4, 9, 16 and 25 hours at 800°C in lab air with no control of humidity. The samples were removed from the oven for ion beam analysis, and were thus subjected to thermal cycling at a rate of ~25°C/min that might have adversely affected the coatings. Composition profiles were determined by comparing SIMNRA computer simulations of the spectra with the original data [19].

Cr volatility was investigated using a transpiration apparatus developed at Lawrence Berkley National Laboratory. To prevent Cr volatility from the uncoated side of the coated coupons, all samples (including uncoated) were first electroplated with ~50μm Ni on one (uncoated) side (Omni Metal Finishing, Inc.). The samples were pre-oxidized in air at 800°C for 2 hours prior to 24 hours exposure to 200 sccm air with 1x10^{4}Pa H_2O at 800°C. The condensate from the effluent gas was then analyzed for its Cr content using ICP-MS.

Economic feasibility assessment

To determine the economic feasibility of FAPSID technology for SOFC metallic interconnects applications, a full-scale FAPSID system model was adopted. Assumptions for coating productivity and costs were made in accordance with SECA manufacturing volume and cost objectives.

Results and Discussions:

Ion beam analysis was used to characterize the oxidation resistance and diffusion characteristics for several candidate bond coatings coming from the CrCoAlYON system. In **Figure 13** we show the results for the effectiveness of a CrAlON bond coat, with no top coat and

three different O/N ratios in the as-grown coatings [25]. The surface of the coating is at the left side in each profile, and the steel substrate can be seen at the right with its characteristic high Fe concentration. The depth scale unit ($1x10^{15}$ atoms/cm^2) is characteristic of RBS measurements, and for this case corresponds to approximately 0.2nm. The vertical scale is a percentage concentration, based on the assumption that the individual concentrations add to 100%. No measurement of hydrogen concentration was made for these coatings. The left column shows the composition for the three coatings as prepared with decreasing oxygen concentration from top to bottom. The O/N ratio for the coatings correlates well with the O/N partial pressure ratio in the chamber during growth. The right column shows the concentration profile for each sample after 25 hours of oxidation at 800°C in a tube furnace with laboratory air.

The bond coats analyzed here behave very differently when subjected to the high temperature oxidizing atmosphere. Sample B9 with about 20% oxygen, as grown, lost almost all of the nitrogen in the coating, and shows only a small amount of Fe diffusion from the substrate into the coating, although it did not diffuse all the way to the surface after 25 hours. Coating C9 contains about 10% oxygen concentration as grown. In marked contrast to sample B9, the nitrogen in sample C9 is almost completely replaced by oxygen after only 1hr of heating at 800°C, and the coating is more susceptible to Fe diffusion from the substrate into the coating. However, this coating did not show any Fe at the surface after 25 hours of heating. For coating D9 there is no oxygen in the as grown sample. The nitrogen in the coating is gradually replaced by oxygen, and is completely lost after 25 hours of heating at 800°C. Diffusion of Fe into the coating begins after only 1 hour of heating, and Fe has reached the surface of the coating after 25 hours of heating. Based on the above results we conclude that introducing oxygen during the coating growth process creates more effective diffusion barriers that slow down the diffusion of Fe from the substrate into the coating. Oxidation of the coatings presumably leads to the formations of Cr_2O_3 and Al_2O_3, as determined from the stoichiometry obtained by RBS. Formation of these oxides during growth, rather than as a result of diffusion during subsequent oxidation, results in a more stable bond coat on these steel substrates.

The adhesion testing results showed in **Figure 4** present the Rockwell C 145kg load indentation marks for as-deposited dual segment (a) and upper segment only coatings (b). The radial crack propagation from the indentation in Figure 4a demonstrates the excellent adhesion of the dual segment filtered arc CrCoON/AlON – filtered arc assisted EBPVD $Mn_{1.5}Co_{1.5}O_4$ coating system. The localized area coating delamination near the indentation in Figure 4b indicates only fair adhesion of the upper segment filtered arc assisted EBPVD $Mn_{1.5}Co_{1.5}O_4$ coating, when deposited without the lower segment coating. These results indicate the substrate/coating interface toughening mechanism provided by the dual segment coating architecture.

Figure 5 shows surface SEM images before and after high temperature oxidation in air at 800°C for over 2,000 hours. **Figures 5a** and **5b** are images of the single, upper segment filtered arc assisted EBPVD $Mn_{1.5}Co_{1.5}O_4$ coating. Figures 5c and 5d are images of the dual segment, filtered arc CrCoON/AlON – filtered arc assisted EBPVD $Mn_{1.5}Co_{1.5}O_4$ coating system. The dual segment coating exhibits significantly finer surface microstructure compared to the single segment coating. This indicates a significant influence of the lower segment coating on the surface morphology and its evolution [27].

ASR testing was performed at both PNNL and MSU using Ag paste for electrical contact. **Figure 6a** shows PNNL data comparing uncoated and dual segment coated Crofer 22 APU. The ASR of the uncoated sample reaches a minimum after ~50 hours, and rises steadily past 15m$\Omega \cdot cm^2$ after 300 hours. The ASR values of the dual segment coating continue to decrease

below 10mΩ·cm^2 after over 800 hours of testing. The spike in this data may be associated with the coating recrystallization process shown in **Figure 5**, which is currently under investigation. **Figure 6b** shows ASR testing results of FA-EBPVD deposited $Mn_{1.5}Co_{1.5}O_4$ compared to $Mn_{1.5}Co_{1.5}O_4$ deposited at PNNL using conventional magnetron sputtering. Differences in ASR behavior between these coating techniques are not significant, with both achieving a similar minimum ASR value of ~5mΩ·cm^2 with ASR slowly rising to ~6mΩ·cm^2 after ~400 hours. As the process times for conventional magnetron sputtered coating is an order of magnitude longer than that for filtered arc-assisted EBPVD coating, the observation of ASR behavior similarity is promising.

ASR testing results at MSU from two coating systems and uncoated Crofer 22 APU are shown in **Figure 7**. Spikes in the data represent thermal cycling events. The two coated samples display lower ASR values compared with uncoated Crofer 22 APU after ~550 hours. ASR values for uncoated Crofer 22 APU continue to rise past 40mΩ·cm^2 after ~1,000 hours, while coated samples display relatively stable ASR behavior, with values below ~25mΩ·cm^2 after ~2,000 hours. The upper segment coating alone had the lowest ASR values, while the dual segment coating exhibited the most ASR stability [27]. The continued growth of a chromium-rich scale under the single, upper segment coating is likely responsible for the continued rise in ASR. The gradual decrease in ASR observed in the dual segment coating is likely due to interfacial and surface evolution during the test. Evidence for Ag paste interaction with both coated and uncoated samples during testing is currently under investigation.

The SEM images in **Figure 8** illustrate TGO scale spallation on uncoated Crofer 22 APU after ~2000 hours oxidation in air. SEM cross section analysis shows an intact scale thickness of ~10μm after this exposure. The poor scale adhesion of the uncoated Crofer 22 APU may be attributed to the aggressive lapping procedure used to prepare the sample surfaces, as this is behavior is not observed on unpolished, uncoated Crofer 22APU coupons after oxidation. This illustrates the effect of roughness and TGO scale adhesion on uncoated steel surfaces.

An SEM image with EDS line profiles for individual elements of the dual segment coating after ~200 hours oxidation in air at 800°C is shown in **Figure 9**. The composition of the upper segment layer is 1:1 Mn:Co, with negligible Cr content. The coating appears dense and well-adhered to the substrate material. Co observed in the bottom coating segment can be attributed to both the LAFAD CrCo/AlON coating deposition process and the inward diffusion from the upper FAD/EBPVD Mn-Co-O segment. In comparison, Mn observed in the bottom segment can be attributed to the inward diffusion from the upper coating segment and outward diffusion from the Mn-containing Crofer substrate. The SEM cross-sections in **Figure 10** present dual segment coatings before and after ASR testing for more than 800 hours. EDS elemental maps and line scans show how the bond layer inhibits TGO layer growth. It can be seen that even with a 0.3μm thick bond AlCrO layer the TGO layer growth is considerably blocked. The coating thickness and composition before and after ASR testing remains similar and coating delamination was not observed. Again, negligible Cr content is found at top of the deposited layer, thus demonstrating the coating's effective reduction in Cr surface transport.

The important conclusion resulting from the analysis of the cross-sectional elemental distribution in nanolaminated Co(Mn)CrO/CrAlO coatings indicates that after long term oxidation, the nanolaminated architecture disappears, and is replaced by a fine-grained, polycrystalline structure [27].

Figure 11 displays Cr volatilization results from single upper segment $Mn_{1.5}Co_{1.5}O_4$ coated and uncoated Crofer 22 APU. The coated sample shows a fifteen-fold decrease in Cr

volatility. SEM/EDS surface analyses after Cr volatility testing indicate that Cr-rich areas were present on uncoated areas (backside and near edges) of coated sample coupons. Coating damage and resulting Cr exposure is suspected to be caused by the Ni plating process for the uncoated side, as seen in the EDX map shown in **Figure 12**. Cr diffusion through the Ni plating is also a possibility. Two-sided coated coupons are currently under investigation to mitigate these effects [23].

Conclusions:

Results obtained during Phase I of the project indicate that nanolaminated structure of the coating does not substantially improve the performance during long-time, high temperature exposures. This resulted in the decision to change the coating design from nanolaminated to a nanocomposite, consisting of atomically mixed AlCrO base phases responsible for high adhesive and cohesive toughness and chromium retaining properties of the coating and MnCoO base phases responsible for high electronic conductivity of the coating at high temperatures up to 800°C. High deposition rates achieved in the LAFAD process both for AlCrO base and CoMnO base oxiceramic coatings allow this monolayer nanocomposite coating to be deposited using the unidirectional LAFAD vapor plasma source alone without the need to combine it with other conventional deposition techniques (e.g. magnetron sputtering, EBPVD, thermal evaporation etc.).

Phase II work

During Phase II of the project, the efforts were dedicated to deposit the nanocomposite coating of the CoMnTiCrAlYON elemental system by unidirectional LAFAD vapor plasma deposition process. The coating has demonstrated high adhesive and cohesive toughness in high temperature cycling up to 800°C, chromium retention and high electronic conductivity properties when deposited on ferritic stainless steel substrates of different geometries.

Experimental methods:

Coating deposition method:

During Phase II of the project, all coatings were deposited using one unidirectional LAFAD vapor plasma source. The optimized LAFAD source at ASE's R&D facility in Bozeman MT has demonstrated high deposition rates which makes this available to deposit the multi-elemental ceramic coatings of CoMnTiCrAlYO(N) composition which were selected as the base coatings for this project. Due to the high LAFAD rates, it was not necessary to combine the LAFAD process with any other conventional PVD processes. Using one LAFAD source instead of the hybrid FAD/EBPVD system that was evaluated during Phase I makes the coating deposition process more robust, simple and economically viable for deposition of protective coatings on metallic IC of SOFC units.

The typical LAFAD plasma processing parameters used in most of the deposition trials reported in this work include the following steps: after pre-heating to 300-350°C using a radiant heater array, the substrates were subjected to fifteen or twenty minutes of ion cleaning at an Ar pressure of 0.8 mTorr in an argon auxiliary arc plasma generated by the LAFAD source with the

deflecting magnetic field turned off. After this step, a short (two to three minute) high voltage metal ion etching step was performed by subjecting the rotating substrates to 100% ionized metal vapor plasma generated by the LAFAD source, while applying -800 to -1000 volts of bias to the rotating substrate table. These two pre-deposition plasma-processing steps are especially important to secure coating adhesion and stability at the coating-substrate interface. The rotation speed of the substrate turntable used in these LAFAD plasma processing trials ranged from 9 to 16 RPM. The substrates to be coated can be installed on single rotation (SR) or double rotation (DR) stations located along the outer perimeter of the turntable. In SR mode, the substrates are rotated around the axis of the turntable with their front surface facing the chamber walls. In DR mode, substrates are subjected to double rotation around satellite station axes as shown schematically in **Figure 2**.

After the metal ion-etching step, the LAFAD coating deposition starts. During deposition of ceramic or cermet coatings, an ultra-thin metallic bond layer is deposited first to further improve the coating adhesion. The metal coatings are deposited in argon, while during deposition of nitrides or oxiceramic layers, a reactive gas (nitrogen and/or oxygen) is added to the processing chamber, forming a reactive gaseous plasma atmosphere. Note that during deposition of near dielectric oxiceramic and oxinitride coatings during Phase II of this project, a 13.56 MHz RF generator was used as a substrate bias power supply, while Phase I coating deposition processes, an MDX-II (Advanced Energy) power supply, coupled with their Sparcle-V accessory, was used as a DC bias power supply. The substrate bias during deposition of most of the conductive coatings reported in this work was -40V, while during deposition of oxiceramic and oxinitride coatings the autopolarization bias potential ranged from -40 to -100 V.

Substrate materials:

Substrate materials were similar to those of Phase I, including ferritic stainless steels (Crofer 22APU, 430 and 441). Additionally, FSS SOFC(IC) specimens were provided by VPS.

Coating properties characterization:

Coating properties were characterized as a function of high temperature exposures as described in the Phase I section. Additional testing was performed at University of Dayton Research Institute, VPS and elsewhere.

Results and Discussions:

Some of the more promising ASE coatings identified so far are LAFAD nanostructured coatings from the MCrAlYO system (where M = Co, Ti, and/or Mn). These coatings are designed to function as effective barriers, blocking both inward and outward ionic diffusion, while providing adequate electronic conductivity through the coating thickness. The transition metal dopants are selected to increase high-temperature electronic conductivity by forming nanocomposite thermistor-like oxicermets. An extensive matrix of LAFAD coatings have been successfully deposited with excellent adhesion to various FSS substrates under consideration for SOFC(IC)s. Other hybrid coating deposition methods, employing filtered arc assisted thermal resistance evaporation and filtered arc assisted electron beam evaporation are also being explored. During the reported period of time, ASE's efforts were focused on optimization of the LAFAD source to increase productivity while at the same time further reducing the density of defects in the coatings. The optimized LAFAD source is now capable of depositing nanocomposite MCrAlYO oxiceramic coatings with deposition rates exceeding 6 μm/hr on

substrates installed on the rotatable 0.5 m diameter turntable of the FAPSID coating system. At the same time, the density of defects dropped at least an order of magnitude. These coating properties are favorable both for high thermal-mechanical stability under long term thermal cycling conditions and for chromium retention.

Chromium volatility assessment was made at MSU using modified transpiration apparatus [23]. **Figure 14** presents a summary of Cr volatility results from uncoated and LAFAD TiCrAlYO coated FSS. The graph displays the cumulative amount of Cr collected during the test. The uncoated FSS continues to volatilize Cr throughout the test, while the coated specimen demonstrates negligible Cr volatility after the first 24 hours. This coating contains ~12at% Cr; however, the Cr is apparently sequestered in a solid solution with complex Al-containing oxides, which agrees well with thermochemical modeling [26].

Thermochemical modeling, using the advanced "TERRA" thermodynamic equilibrium calculation software with solid solution considerations, is being used to estimate phase composition of multielemental oxiceramic coatings and their interactions with SOFC-IC operating environments. The results of thermodynamic modeling of Cr volatilization from TiCrAlYO coating in SOFC simulated environment as a function of Al_2O_3 content are shown in **Figure 15**. It can be seen that an ideal chromia/alumina solid solution can be credited for substantial reduction of the volatilization rate, but cannot explain the nearly complete inhibiting of chromia volatilization from the TiCrAlYO coatings. Kinetic mechanisms, such as formation of Al_2O_3 surface layers, have to be considered for better explanation of this phenomenon.

Evaluations of the first set of nanocomposite coatings have demonstrated nearly the same or even better structural and morphological properties in comparison with the coatings of similar compositions deposited by LAFAD+EBPVD hybrid process during Phase I. The best performance of these coatings was observed with LAFAD nanocomposite (amorphous/nanocrystalline) coatings (~2μm) containing Co, Mn, Al, Ti, Cr and Y oxides (and solid solutions thereof) on 430SS. These coatings appear to combine the proven benefits of Co/Mn-oxide spinels, e.g., low ASR, decreased thermally-grown oxide growth rates, cathode compatibility, with the known diffusion-barrier properties of Al and Cr oxides. Three of these coatings are presented in **Table 1**. Note: the coating architecture in these coatings had the nanolaminated structure produced by exposing the rotating substrates in turn to vapor plasma generated by two opposite primary DCAD sources with different targets, as was described above.

Table 1. Three promising LAFAD coatings

Coating Designation	LAFAD Targets	Approximate Composition (at%) All <1%Y; balance O
TiCrAlYO	TiCrAlY/CrAlY	23Al - 14Cr - 3Ti
CoCrAlYO	CoCrAlY/CrAlY	18Al - 14Cr - 12Co
TiMnCoCrAlYO	CoMn/TiCrAlY	12Mn - 10Al - 9Cr - 3Ti - <1Co

Figure 16 displays ASR values of three of these coatings in contact with LSM at 800°C in air. ASR values for each coating decrease from initial values. This phenomenon has been

attributed to coating evolution, e.g., recrystallization, and outward transport of Mn from the steel through the coating, and was discussed in previous reports and in published literature. The lowest ASR values are realized with the Mn-containing coating, e.g., "TiMnCoCrAlYO", which also demonstrates excellent thermal stability [26].

Figure 17 presents cross-sectional SEM images of coated and uncoated 430 SS after 1,500 hours of ASR testing with LSM contact. Beginning in the left, upper corner and moving clock-wise are: the TiCrAlYO coating; the CoCrAlYO coating; the uncoated 430SS; and, the TiMnCoCrAlYO coating. All of the coatings have retained their as-deposited ~2μm thickness through the 1500 hour ASR test, with some exhibiting compositional stratification (Mn-rich surface crystallites above amorphous alumina base-layer). During the same exposure, the uncoated 430SS (lower right corner) has evolved a TGO layer of >10μm thickness in some regions, with other regions of reaction with LSM (presumably forming $LaCrO_3$).

It was found that some coatings have been observed to retain their as-deposited amorphous structure after more than 1,500 hours exposure in 800°C air demonstrating high thermal-chemical stability of this coating design during high temperature exposure. **Figure 18** illustrates this phenomenon with TiCrAlYO coatings (~3μm) with surface and cross section SEM images of the coating before and after 1,500 hours in 800°C air. The top images show the coating's amorphous surface structure, which has been largely unchanged during the exposure. The bottom images show the coating cross section, which shows some evidence of local outward Mn transport, which appears to have initiated surface crystallite formation.

Table 2. Primary DCAD source targets usage.

Left/Right primary DCAD targets	Left/Right targets total current, ampere	Left/Right targets erosion rate, g/hr
Ti(new)/Ti(new)	140/140	32.2/32.8
Ti(new)/Ti(new)	200/200	73.9/74.5
Ti(used)/Ti(used)	200/200	54.9/55.8
Cr(used)/Cr(used)	200/200	21/20
Ti(used)/Cr(used)	200/200	50.2/21.6
Ti(used)/Cr(used)	140/200	30.5/15.7
Ti(used)/Cr(new)	140/200	35/17.6
TiCrAlY (new)/CoMn(no data)	120/100	44.12/(no data)

The highest productivity of the LAFAD process was demonstrated during the deposition of AlCrO(N)-based multi-elemental oxi-ceramic and oxinitride coatings. This can be attributed to the influx of the oxygen and/or nitrogen atoms conveyed from the metal gaseous plasma to the substrate surface. In case of AlCrO base coatings, the Me_2O_3 corundum phase is prevailing. Therefore for each depositing pair of Al or Cr atoms, three oxygen atoms will be added from the reactive gas atmosphere, which will inflate the coating thickness even more than that of CrN, TiN or AlN coatings. In addition, the primary cathode targets with a high concentration of aluminum have a greater evaporation rate than aluminum-free targets, as can be seen from **Table 2**. The characteristic target evaporation rates in LAFAD process for targets made of different metals and alloys are also presented in **Table 2**. The deposition rate in the LAFAD process also depends on the target material and the condition of the target surface as in any other process using vacuum arcs [5]. The evaporation rate of titanium targets in a vacuum arc process exceeds the chromium evaporation rate by almost a factor of two as shown in **Table 2**. The evaporation

rate of used targets drops by 20 to 25% depending on the usage time and arc current. This can be explained by a reduction of the target evaporation rate when the target is eroded; its front evaporation surface, which gets all the energy influx conveyed from the arc plasma, moves backwards and the distance between the water-cooled back of the target and the front surface of the target (where the evaporation is actually taking place) diminishes. This results in a dramatic decrease in the temperature of the front evaporation surface of the cathode target, which in turn leads to decrease in evaporation rates. It was shown that, in the case of titanium targets, the evaporation rate decreases by a factor of two when the temperature of the front evaporation surface of the cathode target decreases from 800°K to 390°K [28,30].

Table. 3. Coating composition and mechanical properties.

Item#	Primary cathode target composition (total arc current per target I_{arc}, A) Left / Right	Coating designation	Average and (Max) rate over 500cm dia x15cm tall deposition zone, μm/hr	Average and (Max) thickness over 500cm dia x15cm tall deposition zone, μm	RMS Roughness Pre- (Post Deposition), μm*	Hardness/ Elastic Modulus, GPa	Notes
1	Ti20Cr30Al48Y2(120)/ Ti20Cr30Al48Y2(120)	Ti11Cr26Al15Y1 N42(O4)-SL**	(6.96)	3.47 (2.99)		48 / 591	
2	Ti20Cr30Al48Y2(140)/ Ti20Cr30Al48Y2(140)	Ti5Cr19Al21Y1 O54-SL	5.25 (6.3)	(12.6)	0.02/0.07	30 / 290	Figure 19
3	Ti20Cr30Al48Y2(140)/ CoCrAlY(120)	Co9Ti4Cr18Al18 Y1O49-SL	3.06 (3.8)	(4.24)	0.02/0.05	27 / 255	
4	Ti20Cr30Al48Y2(100)/ Co50Mn50(120)	Co6Mn6Ti3Cr11 Al18Y2O54-SL	3.94 (4.61)	(8.68)	0.02	21 / 243	Figure 20. This coating had a thick insulating TiCrAlYO bond sublayer.
5	Ti20Cr30Al48Y2(100)/ Co50Mn50(120)	Co10Mn6Ti4Cr1 4Al14Y2O50-SL		(3.00)	0.02	21 / 243	This coating did not have an insulating TiCrAlYO bond sublayer.
6	Ti20Cr30Al48Y2(140)/ Ti20Cr30Al48Y2(140)	Ti6Cr17Al23Y1 O48N6-SL	4.79 (4.13)	(7.99)	0.02/0.06	27 / 265	

*Roughness was measured by Dektak 8 precision profilometer on coatings deposited on polished 440A SS

**The concentrations of respective elements by Auger and EDS analysis are shown in at% after each element in coating designation formulae

Figure 19 shows the EDS line scan of a 12 μm thick TiCrAlYO monolayer coating deposited by the unidirectional LAFAD plasma source with two primary opposite DCAD sources #1 and #2 equipped with Ti20Cr30Al40Y2 targets on substrates installed on a rotating turntable of the batch coating system. The results of composition analysis of the nanocomposite

coatings deposited by LAFAD process using either identical or different primary cathode targets are also presented in **Table 3**. It can be seen that the coating compositions of TiCrAlY(O,N) coatings deposited by using the same primary targets closely resemble the respective target composition. **Table 3** also presents basic mechanical properties of MCrAlY(O,N) coatings (M=Ti,Co,Mn) deposited in the LAFAD-500C deposition system on 440A Stainless Steel substrates under various processing conditions. The substrates initially had an RMS surface finish of 0.02 μm, and the substrates were mounted on the turntable in 'single rotation' mode.

The maximum deposition rate of TiCrAlYO coating, deposited without vertical rastering of the plasma flows on substrates located near the center line of the LAFAD source exit window, exceeded 6μm/hr, while the average rate inside of the 0.15 m deposition area around the center line of the LAFAD source exit was 5.25 μm/hr. Similar deposition rates have been achieved for a variety of oxiceramic, oxinitride and nitride coatings based on TiCrAlY system with the addition of Co and Mn, as shown in **Table 3**. It can be seen that the hardness of oxiceramic and oxinitride coatings of this elemental system ranges from 20 to 30 GPa, with superhard properties demonstrated by the single-layer TiCrAlYN nitride coating (see **Table 3**). It was also found that the stress level in these coatings increases with increasing nitrogen content, correlating with the hardness. The EDS line scan in **Figure 20** shows the elemental distribution across a 3μm thick CoMnTiCrAlYO coating deposited during a forty minute deposition time by the LAFAD plasma source with two different primary arc targets: a Ti20Cr30Al48Y2 target installed on the primary DCAD source #1 and a Co50Mn50 target installed on the primary arc source #2. It can be seen that the LAFAD process allows effective mixing of two filtered arc plasma flows generated by primary targets with different multi-elemental compositions to achieve deposition of the complex multi-elemental nanocomposite coatings at high deposition rates. Characteristic parameters of the multielemental nitride, oxinitride and oxiceramic coatings of the MCrAlY(O,N) family deposited on FSS plates simulating the SOFC metallic interconnects are shown in **Table 3**.

Table 4: AES Analysis of reference materials, at%.

Sample	Ti	Cr	Al	Y	Si	Zr	Mn	Co	O	Note
$Ti_{20}Cr_{30}Al_{48}Y_2$	19.8	21.1	48.0	2.5	1.0					AES analysis of the target composition
$Ti_{20}Cr_{30}Al_{48}Y_2$	12.9	5.7	78.1	3.2						Coating deposited in a close proximity to the primary DCAD source
$Co_{50}Mn_{50}$							27.2	72.7		Coating deposited in a close proximity to the primary DCAD source
Sapphire (Al_2O_3)			40.6						59.4	
Anodized Ti (TiO_2)	35.7								64.3	
ZrO_2-Y_2O_3				6.3		28.9			64.8	

Samples of the TiCrAlY and CoMn target materials were also analyzed at UDRI. When the AES results were compared with those for single element standards, the TiCrAlY target had considerably more Al and less Cr than expected. Because of the heterogeneity of this sample, it is questionable whether this could be a suitable standard. The AES analysis of the CoMn target showed that it was Co-rich compared to the expected composition. Since most of the coatings

presented in **Table 3** are oxides, it would be better to use oxide samples as reference materials. Samples of sapphire (Al_2O_3), anodized titanium (TiO_2) and YSZ ($Y_2O_3 – ZrO_2$) were analyzed.

The AES results for all of the reference materials are shown in the **Table 4**. There is reasonable agreement between the EDS and AES results for the coating compositions of sample #4 and #5 (see **Table 3**), with the exception that EDS detects more Mn and less Co in these coatings than AES does. AES may underestimate the Mn content due to spectral overlap between Cr, Mn and Fe AES spectra. AES also overestimates the Cr because the stainless steel substrate (which contains more than 16 at% Cr) is being detected since the film (**Table 3**, item #5) is thin. Since the results for the oxide reference materials were in good agreement with the expected compositions, these were used to quantify the results for the coatings presented in **Table 3**.

Table 5. Mechanical properties of LAFAD MTiCrAlYON coatings after 1500 hrs of oxidation in ASR test environment.

Sample description				Average	Average			
	Post Test	Post Test		Pre Test	Pre Test			
	H	E	Post Test Change	H	E			
Ti5Cr19Al21Y1O54-SL*	26.1 +/-5.4	292 +/-43	no	25	275	(on 440A, PWA and carbide)		
Co9Ti4Cr18Al18Y1O49-SL	4.0 +/-1.2	120 +/-18	yes	27	255	(on 440A)		
Co6Mn6Ti3Cr11Al18Y2O54-SL	1.6 +/-0.9	63 +/-35	yes	20	225	(on 440A)		
TiCrAlYN	5.9 +/-3.5	168 +/-105	yes	46	565	(on carbide)		
Ti6Cr17Al23Y1O48N6-SL	19.7 +/-3.0	218 +/-13	probably not	25	260	(on 440A)		

*As-deposited coating elemental composition is shown after each element in at%

After 1500 hours of oxidation at 800°C in the ASR test environment, the mechanical properties of the coatings were analyzed using nanohardness measurement equipment at ASE. Generally, these samples are too rough to test reliably, and much of the data scatter is likely a result of this. With that said, there seems to be a clear indication on four out of six samples that coating recrystallization and a change of composition occurred, which dramatically affected their hardness and elastic modulus. Pre-test H-E values were not measured on the FSS substrates, so relative comparisons were made to identical coatings deposited on polished substrates; averaged values for pre-test substrates are indicated in **Table 5**. Examples of the hardness vs. depth plots are shown in **Figure 28**. Measured hardness was averaged over a range which equals 5%-10% of the coating thickness (this range can be visualized by the 2 diamond markers on each plot). Samples with Co, Mn and N show a dramatic reduction in hardness as a result of long term high temperature exposure (**Figure 28b**). On the other hand, the mechanical properties of the TiCrAlYO coating did not change (**Figure 28a**), which demonstrates the exceptionally high thermal-chemical stability of this coating. The optical photograph of the Rockwell C 145 kg load indentation mark of this coating after 1500 hrs of ASR test exposure shown in **Figure 29** demonstrates only radial cracks without large delaminations which indicates still reasonably good adhesion of this coating after long term high temperature exposure.

Figure 21 presents ASR data from coatings described in **Table 3.** **T**he ASR values for all of these coatings having a thick TiCrAlYO bond interlayer (**Table 3**, all items except the Item No.5) are prohibitively high for the SOFC(IC) application. **Figure 22** presents ASR data from **Figure 21**, emphasizing the lowest ASR coatings. Although no coating meets the 0.01mΩcm^2 requirement, it is demonstrated through this work that small variations in coating elemental composition result in substantial differences in ASR, thus ASR can be effectively engineered into SOFC(IC) coatings, if the coating deposition system permits elemental-level control, such as is the case for Arcomac's LAFAD system. SEM cross sections with EDS linescans of three of the coatings presented in **Figures 21 and 22** are presented in **Figures 23, 24 and 25**. The coatings all retained their approximate as-deposited thicknesses, with evidence for elemental stratification during the 1500 hour exposure, especially for coatings containing Co and/or Mn as-deposited (**Figures 24, 25**). The EDS linescans in each provide evidence of a Si-rich region near the coating/ FSS substrate interface, suggesting the formation of an insulating SiO_2 phase, which may help explain the increase in ASR observed for most of the coatings after long-term testing. Despite this, the coatings have also retained their as-deposited composition and substantially inhibited oxidation of the underlying FSS, as compared with uncoated FSS. In this respect, the coatings served as excellent and stable diffusion-barriers against oxidizing species, e.g., inward transport of oxygen from air and also outward transport of cations from the FSS substrate.

The best ASR results were obtained on samples made of 441 SS with CoMnTiCrAlYO coating (**Table 3**, item 5) having thickness of 3 μm and deposited with ultra-thin TiCrAlYO bond layer (<50nm). The elemental composition of this coating is shown by EDS line scan in **Figure 20**. It can be seen from the ASR results presented in Figures 21, 22 that this coating has a low ASR <50 mOhm·cm^2, which does not increase noticeably after 1500 hrs of high temperature exposure in contrast with all the other coatings. This nanocomposite multielemental oxiceramic coating can be considered as the most promising candidate for SOFC IC application. Still the optimal thickness and elemental composition of this coating has to be further optimized to meet performance requirement when deposited on actual IC plates. It has to be noted that Al-rich bond interfacial sublayer which is very useful to improve coating adhesion is detrimental to ASR values. Therefore, the adhesion and cohesion toughness of the coating as well as its high temperature thermal-mechanical stability and barrier properties have to be secured via adjustment of coating composition with the balance between AlCrO component responsible for the barrier properties and CoMnO components responsible for electronic conductivity, while keeping the AlCrO rich interfacial sublayer at lowest thickness range. The thickness of the coating has to be also optimized. It can be noted that even with AlCrO based oxiceramic coating as thin as 0.3 μm a considerable improvement of inhibiting the TGO growth was obtained (**Figure 10**).

Figure 26 presents a surface image of a CoMnO coating (Phase I) after 1000 hours in 800°C air, courtesy of VPS. The observed coating delaminatation suggests poor adhesion of this Phase I coating, which may be explained by the nanolaminated architecture of these coatings presented in **Table 1** with sharp boundaries between the neighboring sublayers which can result in cohesive failures. **Figure 27** shows a cross section of a Phase II nanocomposite coating presented in **Table 3** (item 4) tested within a 6-cell stack at VPS. This coating was deposited by mixing TiCrAlY and CoMn plasma flows generated by the primary DCAD sources in the LAFAD process. This coating demonstrated substantial improvement of the adhesion and high temperature thermal-mechanical stability as compared to Phase I coatings due to the interfacial layer resulting from the reaction of the deposited AlCrO rich bond sublayer with steel substrate

and nanocomposite nature of the coating. On the other hand, the presence of the Al-rich bond layer and a relatively high thickness of this coating resulted in increased ASR and poor stack performance. Currently, VPS is testing optimized nanocomposite coating (**Table 3**, item #5) deposited without Al-rich bond layer within SOFC stacks to determine the efficacy of the Arcomac coating strategy developed through this program. As soon we will get the results from this evaluation we will submit it as a supplement to this final report.

Economic feasibility assessment

Regardless of the FAPSID process embodiment, it is assumed that the required coating thickness (as determined through Phase I + II work) will be achieved via a less than half an hour coating deposition process. This process will be designed to accommodate 600 interconnect plates per run. With 300 days operation per year, maintaining 10 daily processes, the productivity estimates are ~0.9 million interconnects per year, sufficient to support ~45MW SOFC stack production. Process consumables include stamped interconnect plates (430 stainless steel -10x10x0.1cm); evaporation targets; electricity and other minor consumables (fluids, gases, etc.). The following cost estimates were assumed: ~$0.10 per interconnect plate as stamped [22]; ~$0.03 per plate for pre-deposition treatment (based on known processes); and $10,000 for evaporation targets and other process consumables, which will support 100 process cycles. Using these estimates, the total processing costs of ~$0.63 per plate are determined. For comparison, the in-line EBPVD process developed at the Fraunhofer Institute in Germany has demonstrated the capability of producing SOFC(IC)-relevant coatings for a cost of approximately five Euros per square meter, which translates to ~$0.08 per 10x10cm SOFC(IC). Arcomac's LAFAD+EBPVD technology is inherently amenable to this industrially-scaled format, and therefore it is likely SOFC(IC) coatings could be prepared for as low as ~$0.10 per plate, given corresponding large-scale SOFC development and demand. This is assuming operation costs only, with fully-automated production.

Although it is generally accepted that PVD techniques require larger capital costs than conventional coating techniques, (e.g., spray or electroplating), considerations of improved compositional and microstructure control, in addition to mitigation of hazardous materials favor PVD techniques for SOFC components applications. In addition, the LAFAD technology in a hybrid combination with conventional magnetron sputtering and EBPVD processes is a promising approach to produce both protective coatings and functional SOFC thin film materials such as insulated seal coatings, YSZ or similar thin film electrolyte, LSM or similar cathode materials and Ni-YSZ anode in one vacuum cycle. A professional, detailed economic analysis, which includes life-cycle costs of different coating technologies, and their operational/safety costs, in addition to their inherent differences in coating composition and microstructure control, is needed to determine which coating technique is favorable for the SOFC(IC) application (regardless of coating composition).

Conclusion:

The continued TGO scale growth observed on ~~the~~ uncoated FSS coupons makes them unsuitable for long-term use as SOFC interconnects. For this reason, it is imperative to develop effective protective coatings. Arcomac Surface Engineering has developed advanced coating deposition processes, to enable the use of inexpensive metallic alloys as interconnect components in planar SOFC systems. Long-term ASR stability of Crofer 22APU has been improved by the use of a two-segment coating architecture: A bottom segment, based on Ti-Cr-

Al-Y-O composition was deposited by unidirectional LAFAD vapor plasma source, while a top segment, based on Mn-Co-O, was deposited by filtered arc-assisted Electron Beam Deposition. In addition to improved ASR stability, the coated samples exhibited much better high-temperature oxidation resistance, along with nearly 100% reductions in Cr volatility. The observed improvements are most likely due to the diffusion-barrier characteristics of the lower segment coating and to the high electrical conductivity and excellent Cr-retention properties of the upper segment coating. It was found that the composition of the FSS substrate also affect the coating performance. For example, when the FSS substrate contains Si, this results in the growth of an insulating SiO_2 sublayer at the coating-to-substrate interface, which is detrimental to the long term performance of the IC plates.

The exceptional high temperature stability was demonstrated by a nanocomposite TiCrAlYO coating deposited by the unidirectional LAFAD vapor plasma source. This coating retains its mechanical properties and high adhesion after 1500 hrs at 800°C in ASR test environment. It effectively inhibits Cr volatilization and TGO scale growth. Since this coating is a poor conductor, nearly dielectric it cannot be used as a protective coating for the FSS ICs without the addition of other elements which can make it a good conductor. This coating can be recommended for a seal of the SOFC bipolar plates. The addition of Co and Mn to TiCrAlYO composition have demonstrated a high promise by forming electronically conductive spinel phases, which are thermal-chemically stable and can survive a long term exposure in the SOFC environment. More work is needed to optimize this promising coating composition and structure, with the optimal thickness expected to be in the range between 0.5-3μm. The high deposition rate of this coating by the LAFAD process which surpasses other conventional vacuum processing technologies makes it a cost effective approach in mass production of SOFC components. In addition, the compatibility of LAFAD process with conventional magnetron sputtering and EBPVD techniques makes it a promising technological platform for developing a continuous in-line vacuum process for manufacturing the entire SOFC cell.

A wide variety of coating compositions and architectures have been investigated to meet SECA's SOFC interconnect performance and cost requirements. A large, industrial-scale, deposition system, offering favorable economics by virtue of its high throughput and advanced hybrid design is currently under development. Preliminary economic evaluations indicate that the cost of these state-of-the-art PVD coatings could eventually drop as low as ~ $0.10 per plate at mass production stage, with the added benefit of much better quality control and drastically reduced hazardous waste production in comparison to conventional coating techniques. Collaboration with Industrial SOFC developers is ongoing in order to evaluate the coated samples under realistic operating conditions.

REFERENCES

1. S.C. Singhal and K. Kendall, High-Temperature Solid Oxide Fuel Cells: Fundamentals, Design and Applications, Elsevier Science, Ltd. 2004

2. P.E. Gannon, C.T. Tripp, A.K. Knospe, C.V. Ramana, M. Deibert, R.J. Smith, V.I. Gorokhovsky, V. Shutthanandan, D. Gelles, **"**High Temperature Oxidation Resistance and Surface Electrical Conductivity of Stainless Steels with Filtered Arc CrAlN Superlattice and/or Multilayer Coatings" in *Surface and Coatings Technology* 188-189 (2004) 55-61.

3. M.Williams, Proceedings of the 7th International Symposium on Solid Oxide Fuel Cells, ed. S.C.Singhal and H.Yokakawa, pp. 3-7,The Electrochemical Society, Inc. Pennington, NJ, (2003).

4. Z. Yang, K. S. Weil, D.M. Paxton, and J.W. Stevenson: J. Electrochem. Soc., 2003, vol. 150 (9), pp. A1188-A1201.
5. Crofer 22 APU "High Temperature Alloy" MSDS No. 8005 June, 2004 ThyssenKrupp VDM
6. Z. Yang, J.S. Hardy, M. Walker, G. Xia, S.P. Simner, and J.W. Stevenson: J. Electrochem. Soc., 2004, vol. 151 (11), pp. A1825-A1831.
7. V.Gorokhovsky, US Pat. No.7,300,559.
8. S. Elangovan, S. Balagopal, M. Timper, I. Bay, D. Larsen, and J. Hartvigsen Journal of Materials Engineering and Performance 13(3) 265-273 (2004).
9. Y.Yoo, M.Dauga, Proceedings of the 7th International Symposium on Solid Oxide Fuel Cells, ed. S.C.Singhal and H.Yokakawa, pp. 837-846, The Electrochemical Society, Inc. Pennington, NJ, (2001).
10. N.Oishi, et.al., Surface and Coatings Tech. 132, 58-64 (2000)
11. M. Kawate, A.K. Hashimoto, and T. Suzuki: Surface and Coatings Technology, 2003, vol. 165, pp. 163-167.
12. O. Banakh, P.E. schmid, R. Sanjines, and F. Levy: Surface and Coatings Technology, 2003, vol. 163-164, pp. 57-61.
13. S. PalDey and S.C. Deevi: Materials Science and Engineering, 2003, vol. A342, pp. 58-79.
14. Y. Larring and T. Norby: Journal of the Electrochemical Society, 147 (9) 3251-3256 (2000)
15. Z. Yang, G. Xia, and J.W. Stevenson: Electrochemical and Solid State Letters, 8 (3) A168-A170 (20005)
16. X. Chen, P. Y. Hou, C. P. Jacobson, S. J. Visco, L.C. De Jonghe: Solid State Ionics (176) 2005 425-433
17. V.I. Gorokhovsky, R. Bhattacharya, and D. G. Bhat: Surface Coatings and Technology, 2001, vol. 140, pp. 82-92
18. W.-D.Munz, T.Hurkmans, G.Keiren, and T.Trinh, J.Vac.Sci.Technol. A 11(5), Sep/Oct 1993 2583-2589.
19. M. Mayer, SIMNRA User's Guide, Technical Report IPP 9/113, Max-Planck-Institut fur Plasmaphysik, Garching, Germany, (1997).
20. J.R. Tesmer, M. Nastasi, Handbook of Modern Ion Beam Materials Analysis, Materials Research Society, Pittsburgh, PA, 1995.
21. R.J. Smith, C. Tripp, A. Knospe, C.V. Ramana, A. Kayani, Vladimir Gorokhovsky, V.Shutthanandan, and D.S. Gelles, J. Mater. Eng Performance, 13 (2003) 295.
22. D. England, (2004) private communication.
23. Collins C, Lucas J, Buchanan TL, Kopczyk M, Kayani A, Gannon PE., Gorokhovsky V.I., "Chromium volatility of coated and uncoated steel interconnects for SOFCs" Surf Coat Technol 201 (7): 2006; (special issue) 4467–70.
24. "Using CrAlN Multilayer Coatings to Improve Oxidation Resistance of Steel Interconnects for Solid Oxide Fuel Cell Stacks," R.J. Smith, C. Tripp, A. Knospe, C.V. Ramana, A. Kayani, V. Gorokhovsky, V. Shutthanandan, D.S. Gelles, J. Journal of Materials Engineering and Performance, Volume 13, Number 3, June 2004.
25. Kayani, A. ; Smith, R.J. ; Teintze, S. ; Kopczyk, M. ; Gannon, P.E. ; Deibert, M.C. ; Gorokhovsky, V.I. ; Shutthanandan, V., "Oxidation studies of CrAlON nanolayered coatings on steel plates" *Surface & Coatings Technology* Volume: 201, Issue: 3-4, October 5, 2006, pp. 1685-1694.
26. Chen, H. ; Lucas, J.A. ; Priyantha, W. ; Kopczyk, M. ; Smith, R.J. ; Lund, K. ; Key, C. ; Finsterbusch, M. ; Gannon, P.E. ; Deibert, M.,V.I. Gorokhovsky, V. Shutthanandan, P.

Nachimuthu "Thermal stability and oxidation resistance of TiCrAlYO coatings on SS430 for solid oxide fuel cell interconnect applications", *Surface & Coatings Technology* Volume: 202, Issue: 19, June 25, 2008, pp. 4820-4824.
27. V.I.Gorokhovsky, P.E.Gannon, M.C.Deibert, R.J.Smith, A.Kayani, M.Kopczyk, D.VanVorous, Zhenguo Yang, J.W.Stevenson, S.Visco, C.Jacobson, H.Kurokawa and S.Sofie, "Deposition and Evaluation of Protective PVD Coatings on Ferritic Stainless Steel SOFC Interconnects," Journal of The Electrochemical Society, v. 153 (10) A1886-A1893 (2006).
28. R.L.Boxman, D.M.Sanders, and P.J.Martin, *Handbook of Vacuum Arc Science and Technology*. Park Ridge, N.J.: Noyes Publications, 1995.
29. V. Gorokovsky, C. Bowman, P.E. Gannon, D. VanVorous, J. Hu, C. Muratore, A.A., Voevodin, Y.S. Kang, "Deposition and Characterization of Hybrid Filtered Arc-Magnetron Multilayer Nanocomposite Cermet Coatings for Advanced Tribological Applications," Wear 265 (2008) 741-755.
30. I. I. Aksenov *et al.,* "Plasma in a stationary vacuum-arc discharge.
Part 2: Effects of integral cathode temperature,'' *High Temp.,* vol. 21, pp. 484-488, 1983.

LIST OF ACRONYMS AND ABBREVIATIONS:

SECA – Solid State Energy Conversion Alliance
SEM – Scanning Electron Microscopy
TEM – Tunneling Electron Microscopy
PNNL – Pacific Northwest National Laboratory
LBNL – Lawrence Berkeley National Laboratory
NASA – National Aeronautics and Space Administration
ASR – Area Specific Resistance
RBS – Rutherford Backscattering Spectroscopy
SOFC – Solid Oxide Fuel Cell
EBPVD – Electon Beam Physical Vapor Deposition
FAD – Filtered Arc Deposition
LAFAD-Large Area Filtered Arc Deposition
LLC – Limited Liability Company
ASE – Arcomac Surface Engineering, LLC
FAPSID – Filtered Arc Plasma Source Ion Deposition
FSS- Ferritic Stainless Steel
LSM-$(La,Sr)MnO_3$
DCAD- Direct Cathodic Arc Deposition
UDRI- University of Dayton Research Institute
VPS- Versa Power Systems
XRD- X-ray diffraction
EDS- Electron Dispersion Spectroscopy
TGO- Thermally Grown Oxide
ICP-MS- Inductively Coupled Plasma Mass Spectrometry
IC- interconnects
RMS-Root-Mean Square
H/E Hardness –to- Elastic Modulus Ratio
MSU- Montana State University
RF- Radio Frequency
SS- Stainless Steel
AES- Auger Electron Spectroscopy

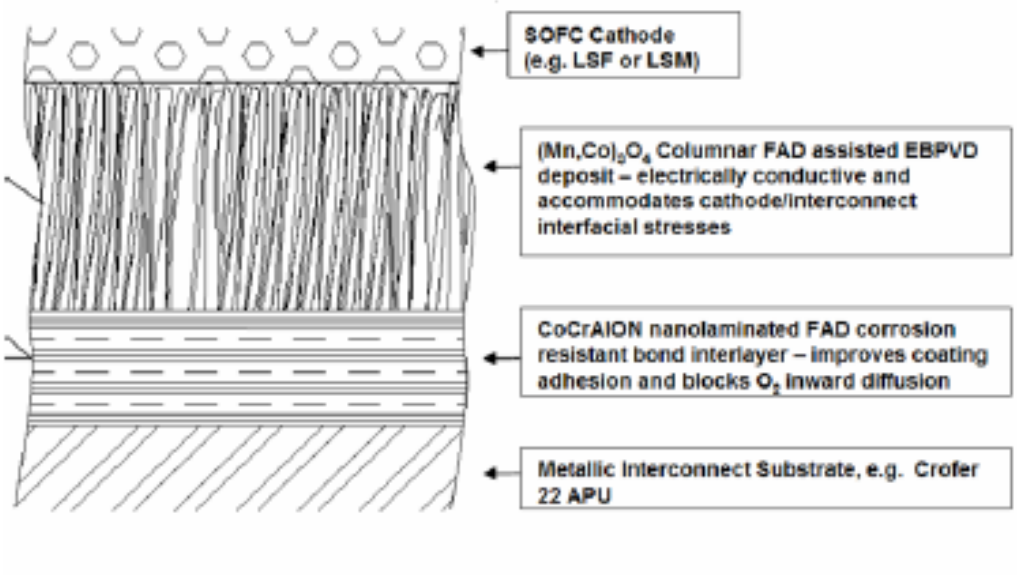

Figure 1. Dual segment, hybrid coating approach.

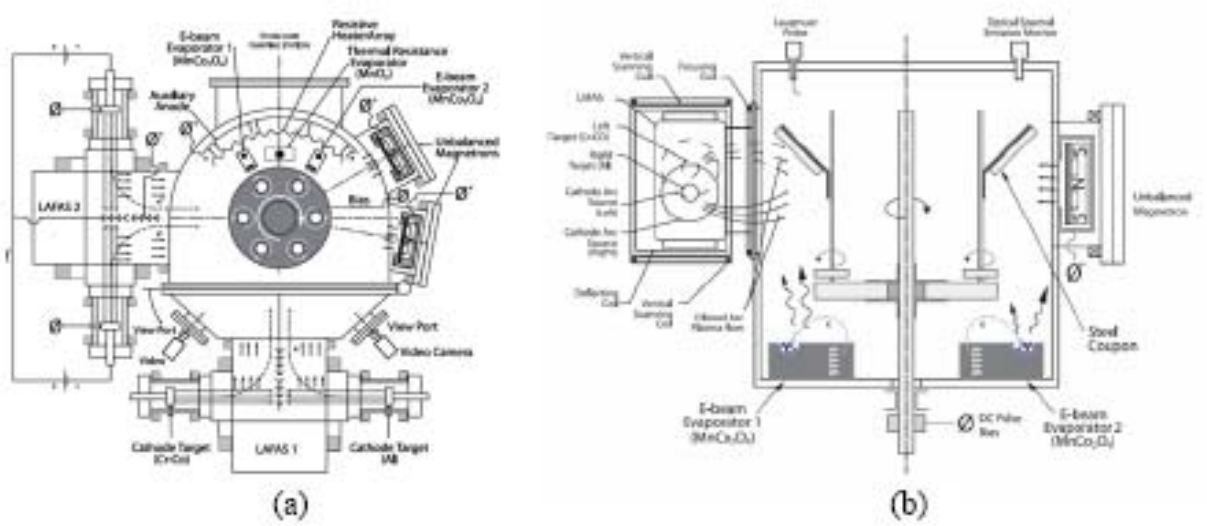

Figure 2. Schematic illustration of the FAPSID surface engineering system, showing (a) top view; and (b) side view.

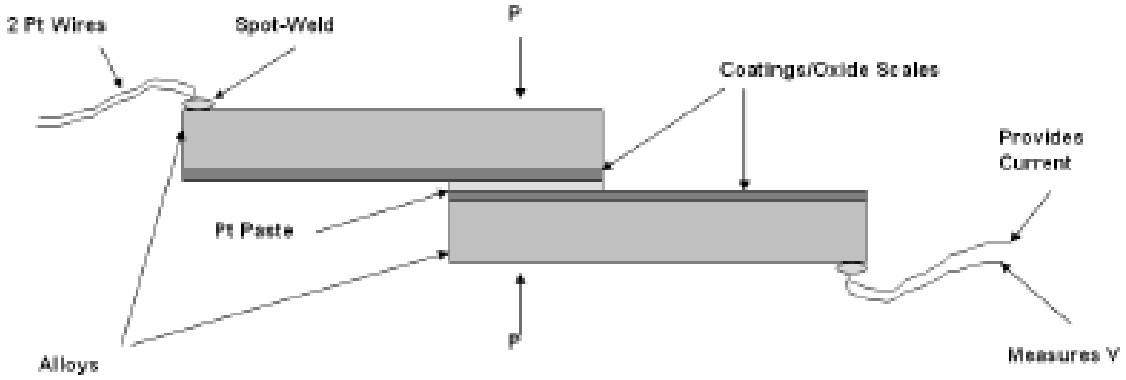

Figure 3. Four-point probe Area Specific Resistance measurement schematic.

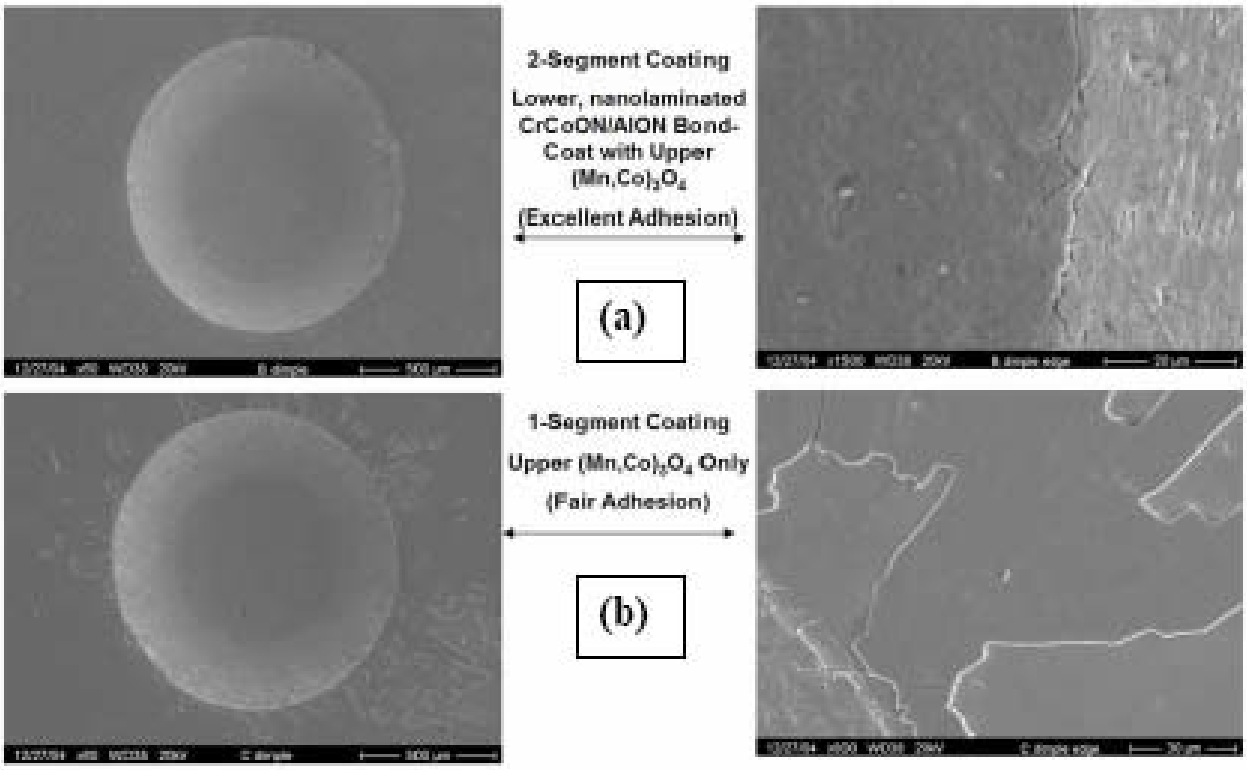

Figure 4. Adhesion (indentation) testing of as-deposited: (a) dual; and, (b) single segment coatings on Crofer 22 APU.

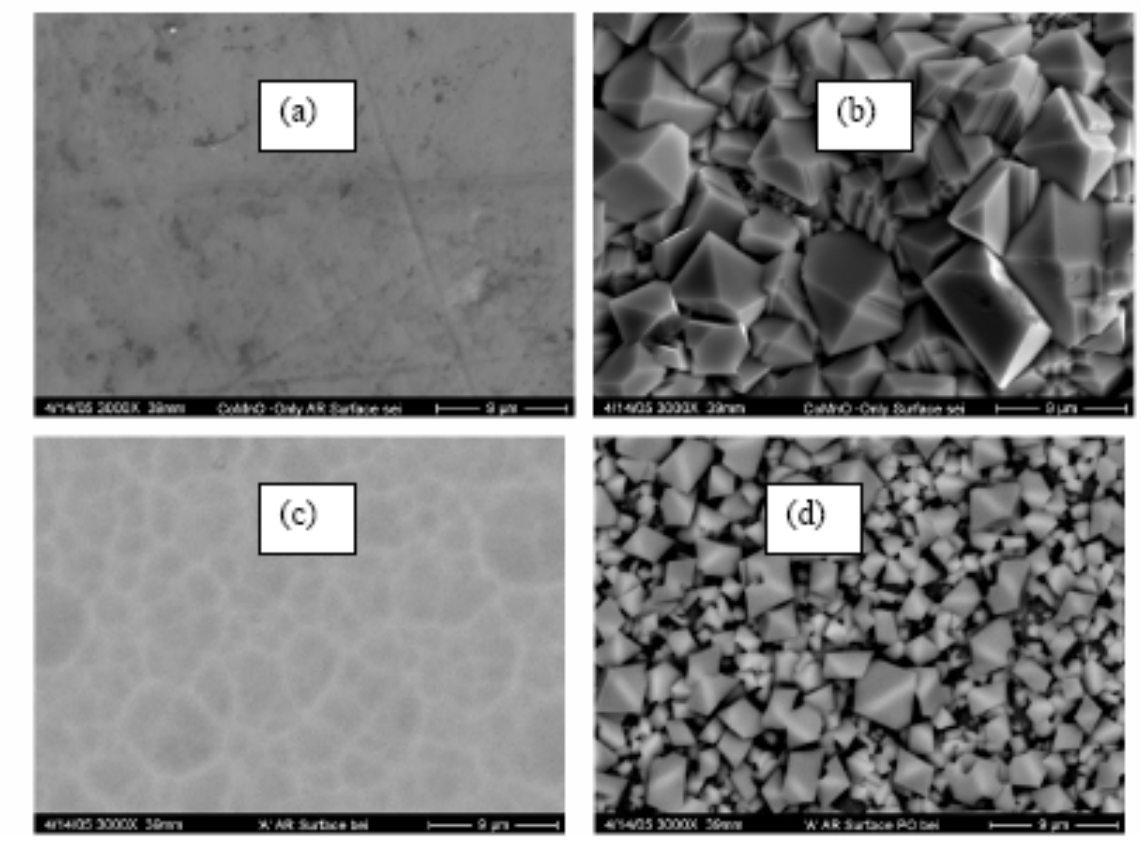

Figure 5. Surface SEM images demonstrating coating recrystallization behavior: (a) as deposited, amorphous or ultrafine polycrystalline $Co_{1.5}Mn_{1.5}O_4$ single segment coating; (b) $Co_{1.5}Mn_{1.5}O_4$ single segment coating post 2,000 hours oxidation at 800°C; (c) as deposited, amorphous or ultrafine polycrystalline CrON/AlON + $Co_{1.5}Mn_{1.5}O_4$ dual segment coating; and (d) CrON/AlON + $Co_{1.5}Mn_{1.5}O_4$ dual segment coating post 2,000 hours oxidation at 800°C.

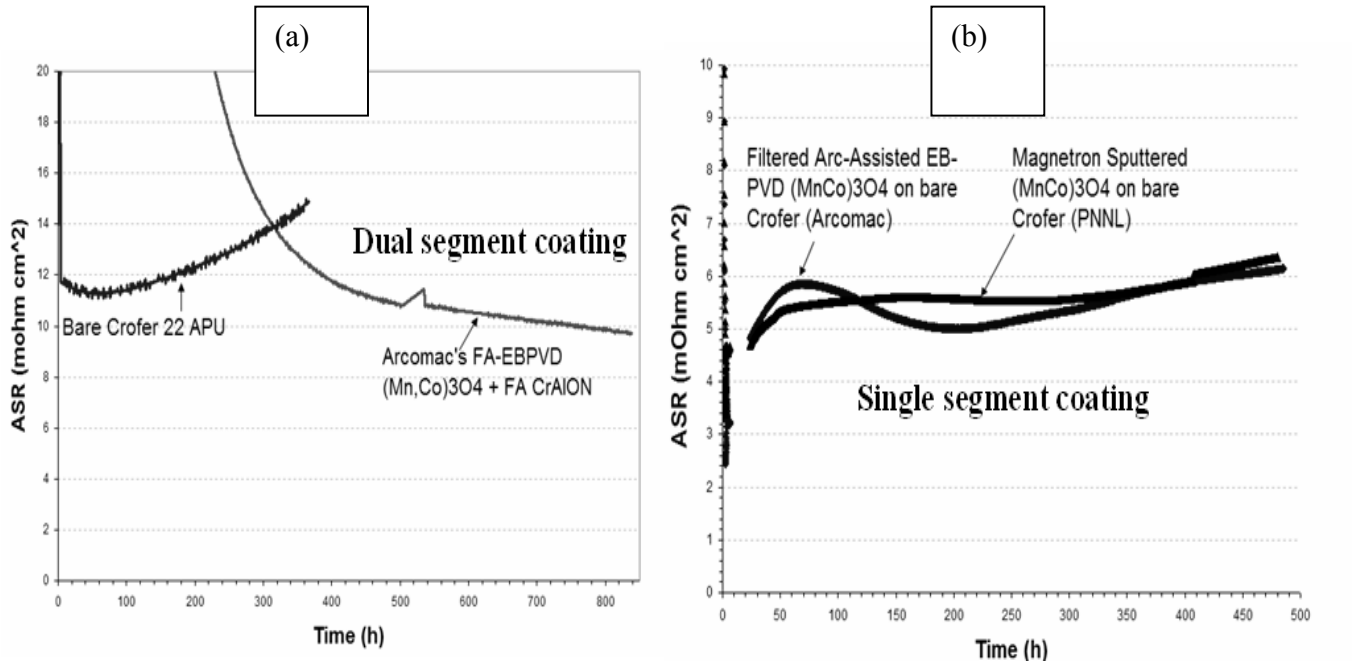

Figure 6. ASR testing results from PNNL.

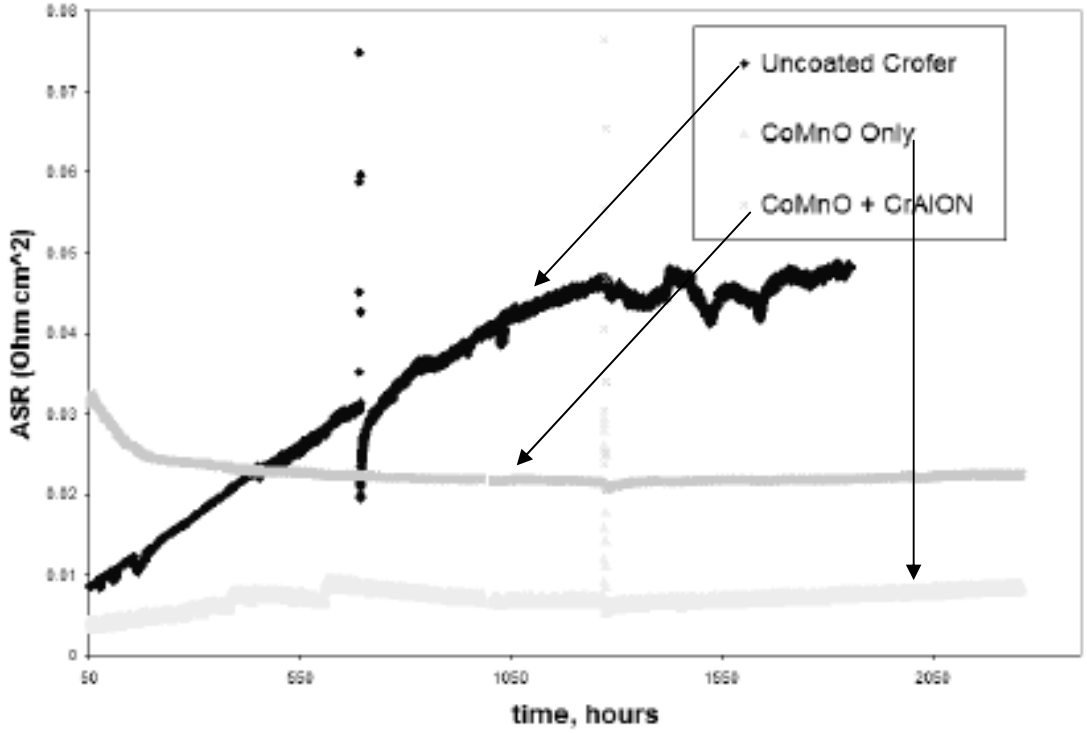

Figure 7. ASR testing results from MSU.

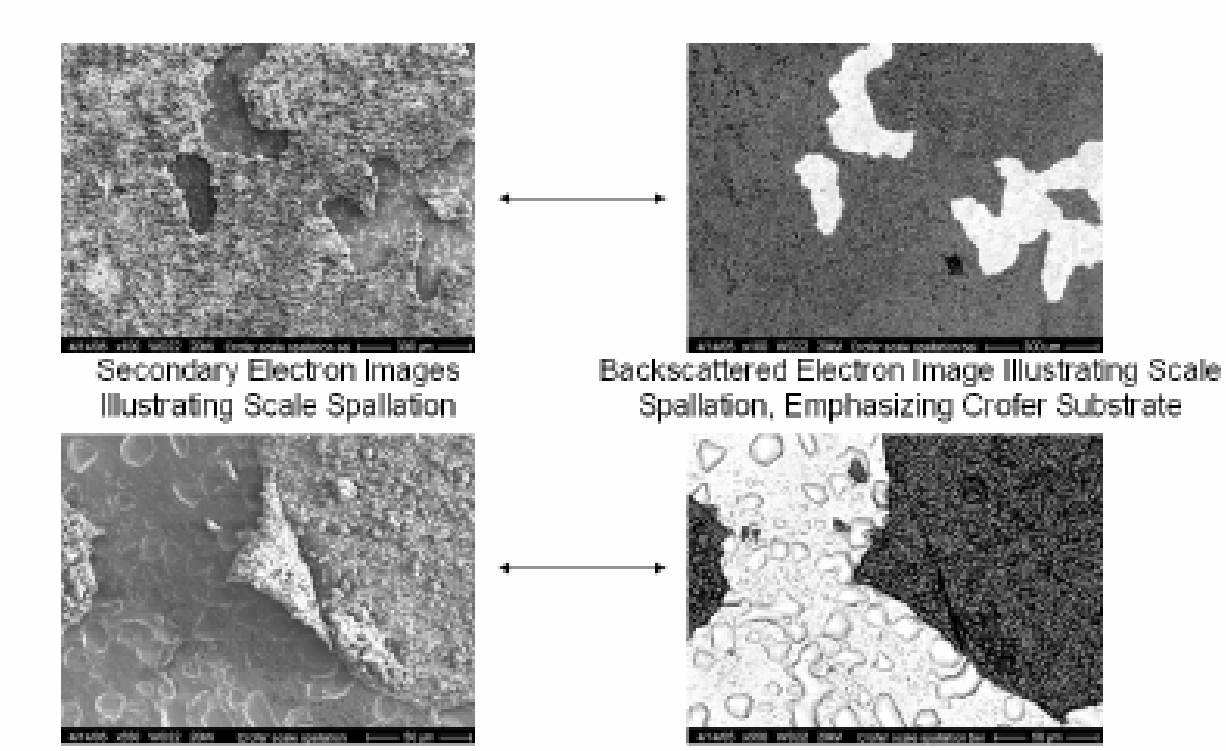

Figure 8. SEM images of TGO scale spallation on uncoated Crofer 22 APU after 2,000 hours in air at 800°C.

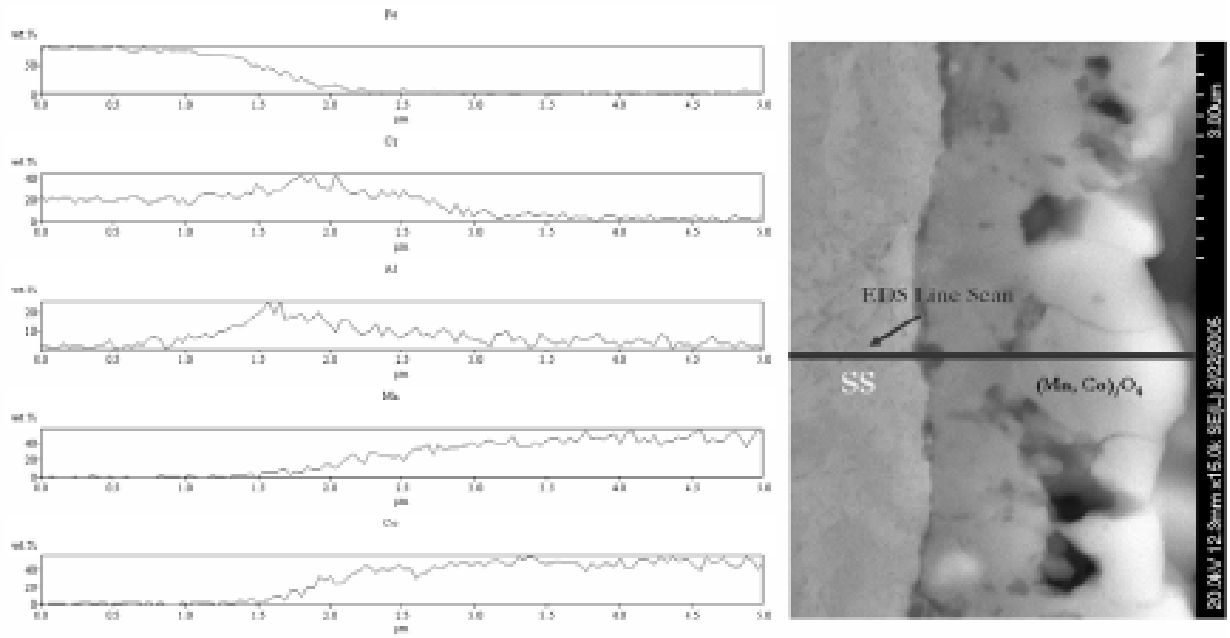

Figure 9. SEM/EDS Cross section of dual segment coating (CrON/AlON + $Co_{1.5}Mn_{1.5}O_4$) after 200 hours oxidation in air at 800°C.

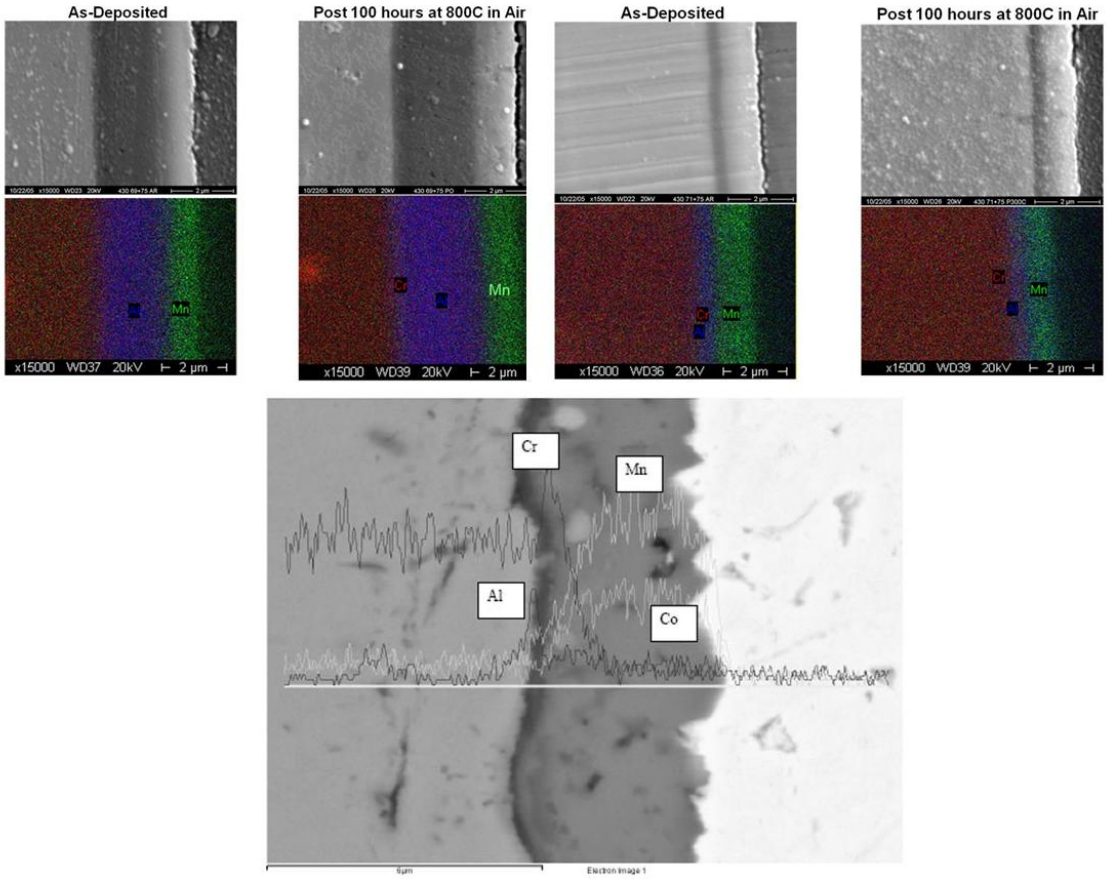

Figure 10. SEM/EDS cross sections of dual segment coating before and after oxidation in 800C air. Top left: 3.0um CrAlYO + 1 um MnCoO: no chromia TGO scale growth showing no substantial change in coating structure after high temperature exposure. Top right: 0.3um CrAlYO + 1 um MnCoO: still no chromia TGO scale growth and no substantial change in coating structure after high temperature exposure. Bottom: SEM/EDS line scan of dual segment coating after 800 hours ASR testing with Ag contact.

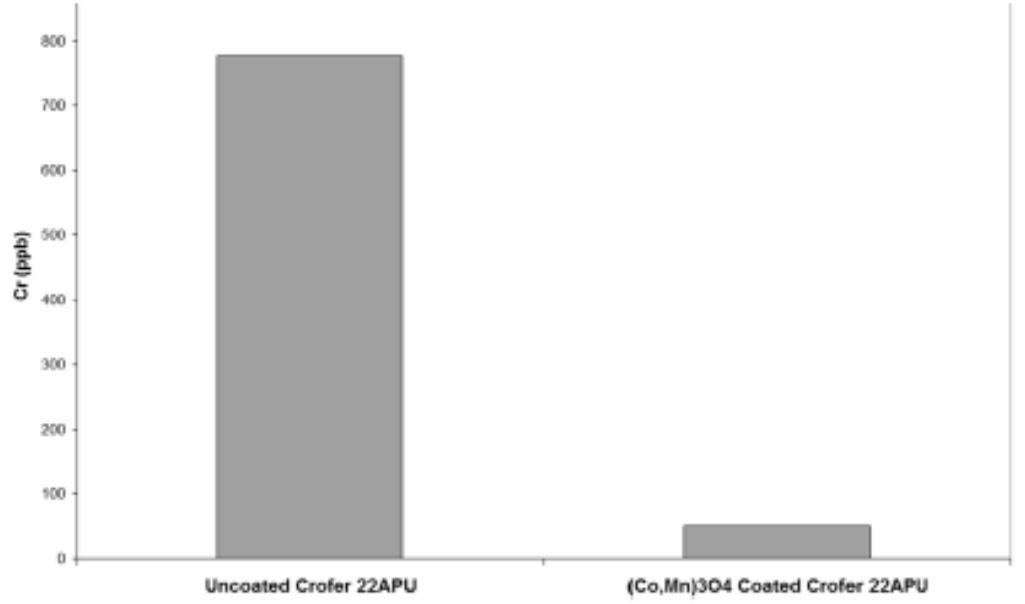

Figure 11. Cr volatility results from coated and uncoated Crofer 22APU sample coupons.

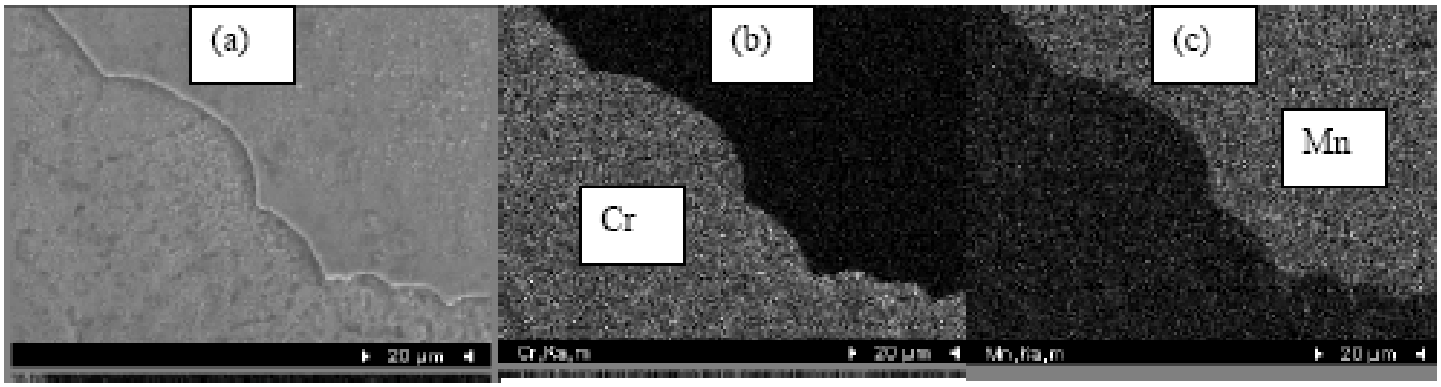

Figure 12. SEM surface image (a) and EDS elemental maps (b, c) of $Co_{1.5}Mn_{1.5}O_4$ coated Crofer 22APU, damaged near edge of sample coupon.

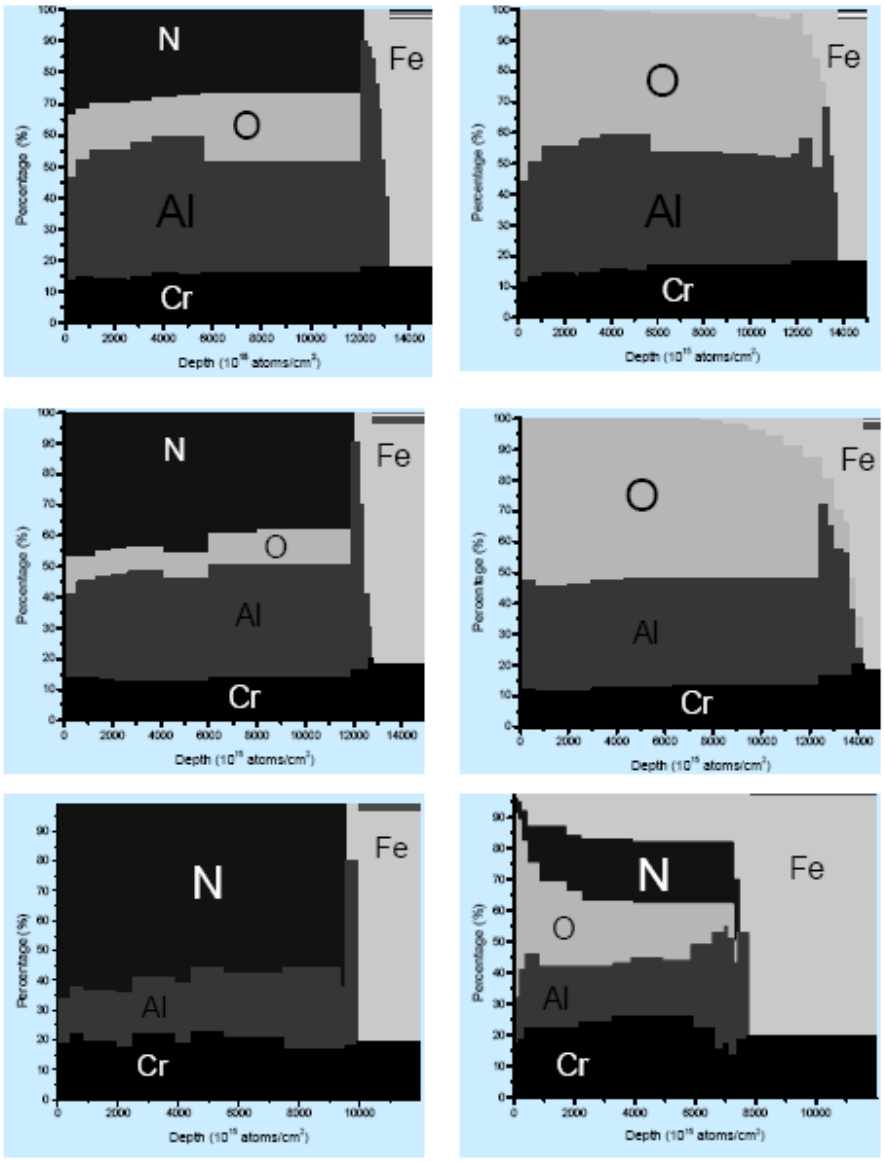

Figure 13. Profiles of concentration versus depth for three samples with decreasing O/N ratios (top to bottom) before (left) and after (right) 25 hours oxidation at 800°C.

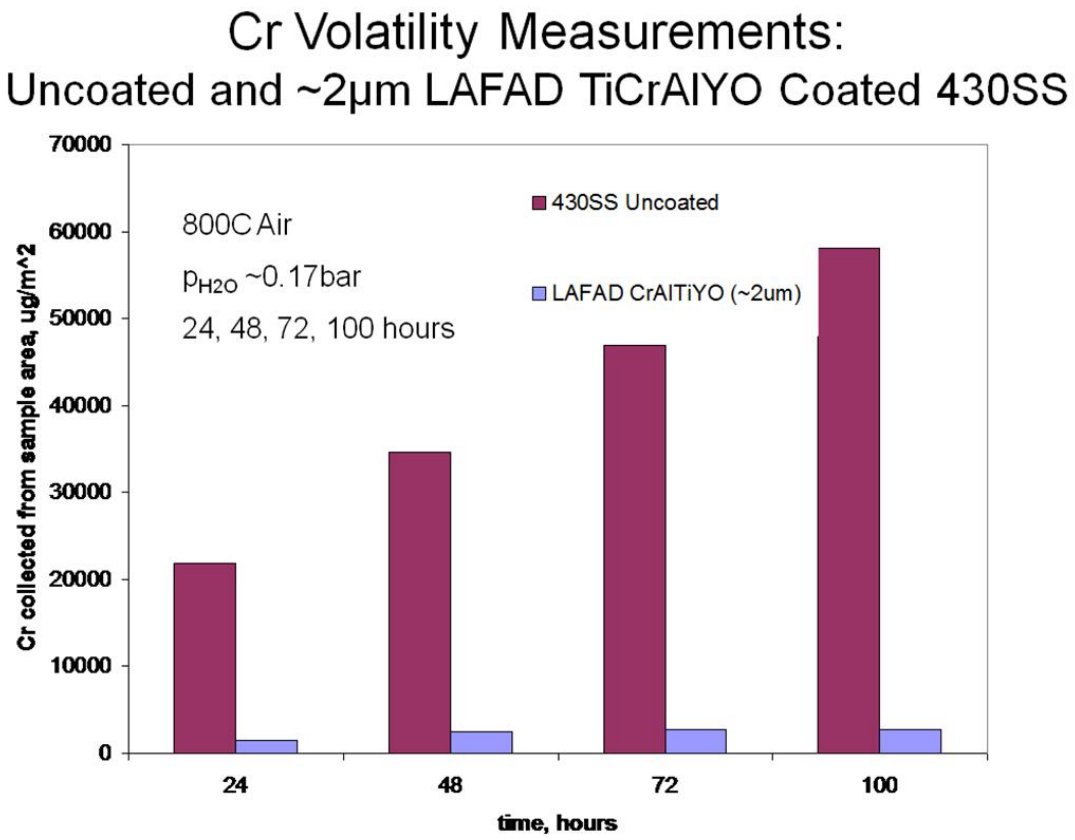

Figure 14. Cumulative Cr volatilized from uncoated and LAFAD coated FSS 430.

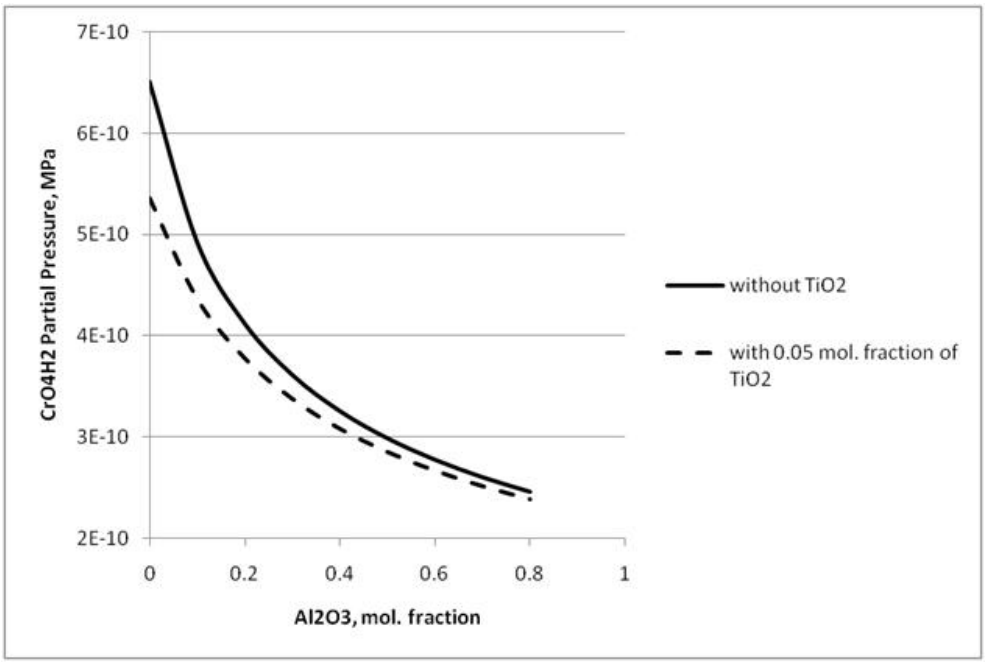

Figure 15. Thermochemical modeling of LAFAD TiCrAlYO coatings to help explain observed reduction in Cr volatility.

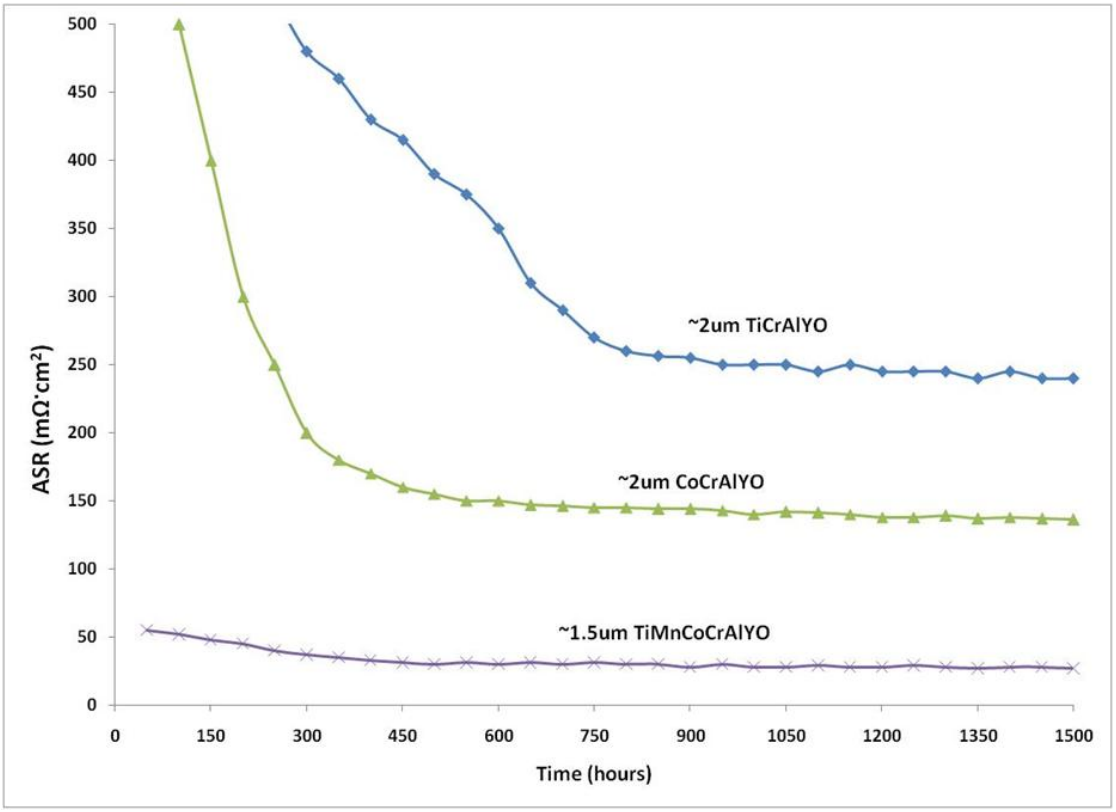

Figure 16. ASR measurements vs. time (LSM contact in 800°C air).

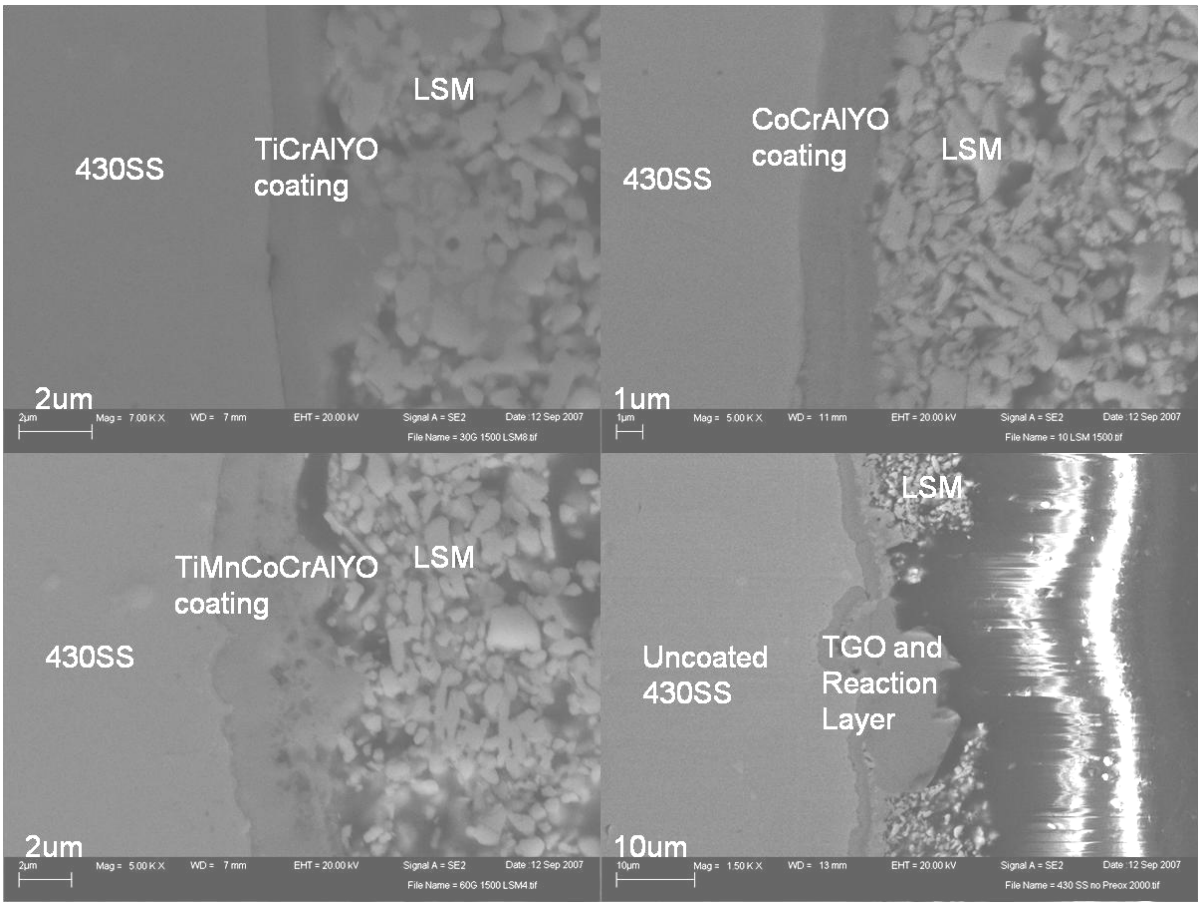

Figure 17. Cross sectional SEM images of LAFAD coated and uncoated 430SS subsequent to 1,500 hours ASR testing in contact with LSM at 800°C in air.

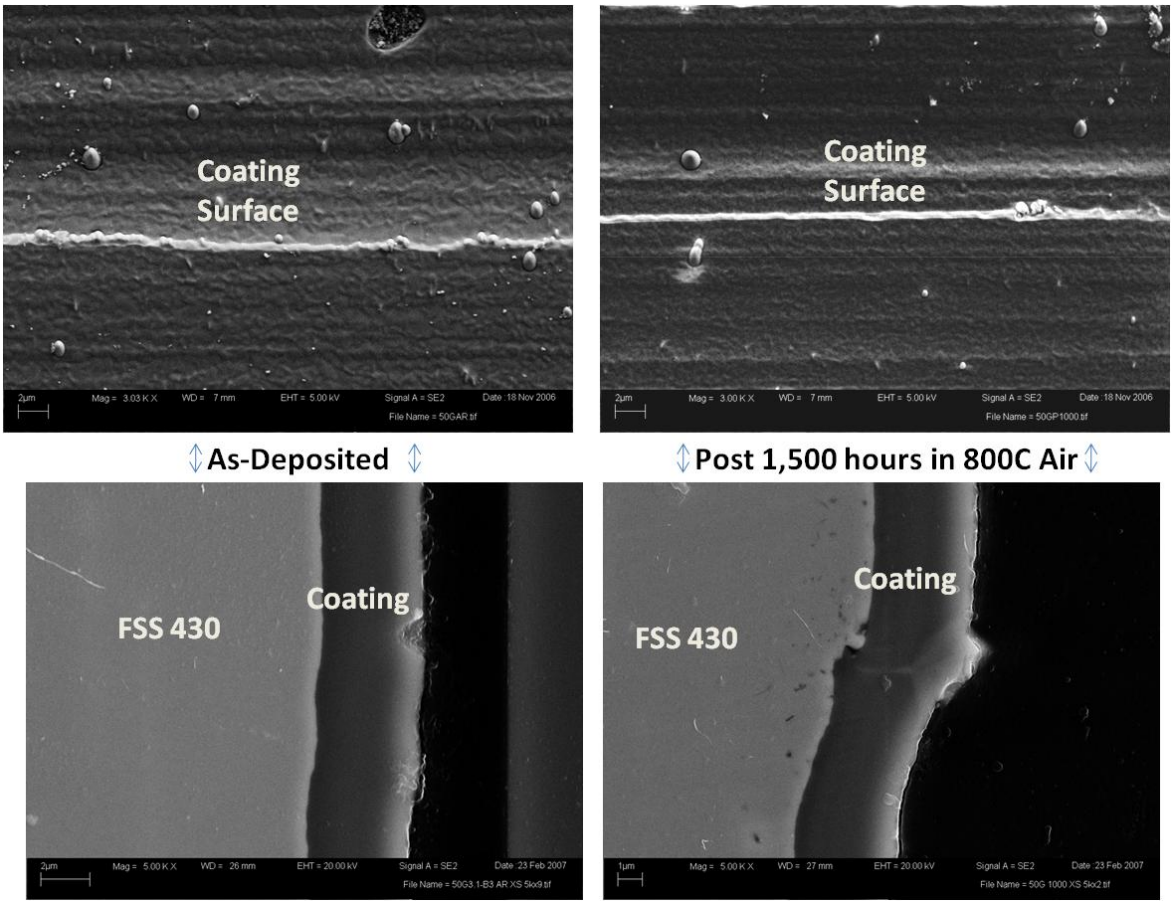

Figure 18. SEM surface and cross section images of 3µm thick LAFAD TiCrAlYO coating (see coating ID in **Table 1**) before and after 1,500 hours in 800°C air.

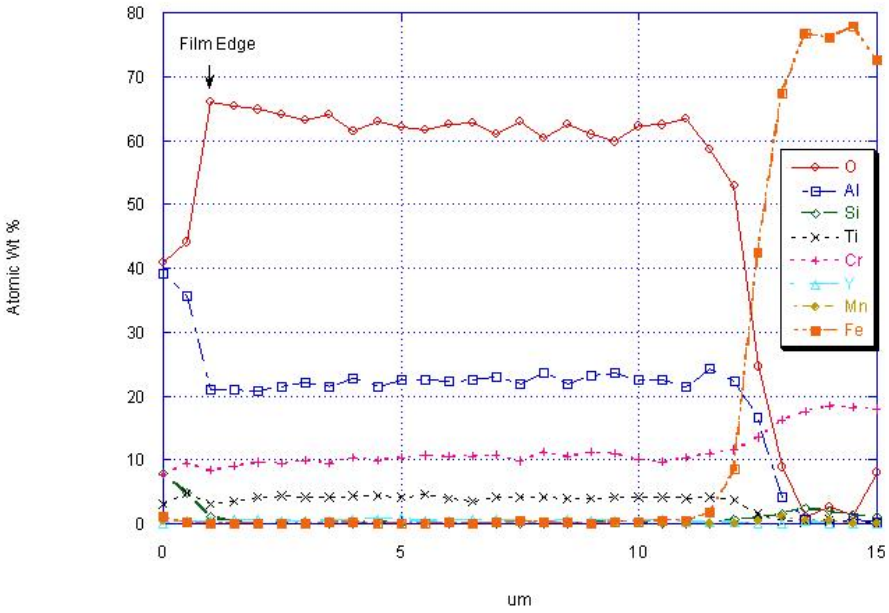

Figure 19. EDS line scan accross 12 um thick TiCrAlYO oxiceramic coating as deposited (see sample ID in **Table 3**, item 2).

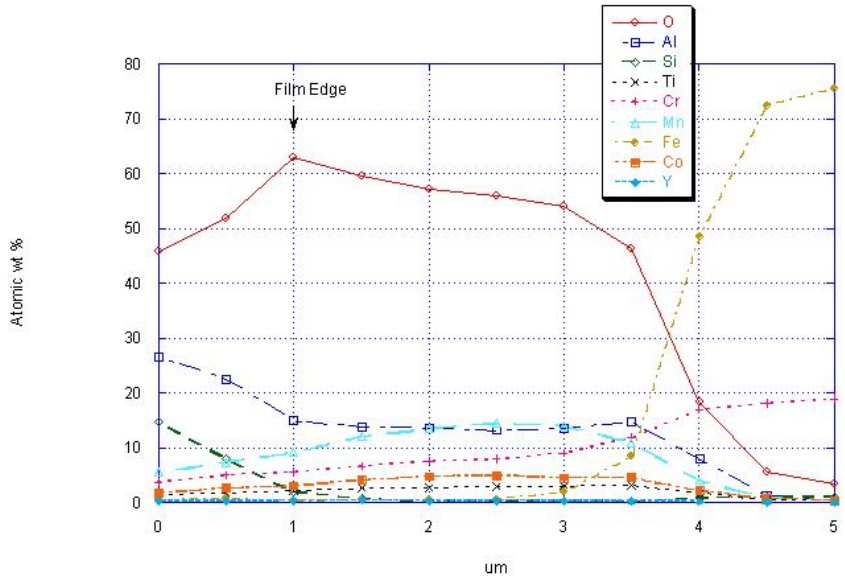

Figure 20. EDS line scan across 3 um thick CoMnTiCrAlYO coating as deposited (see sample ID in **Table 3**, item 5).

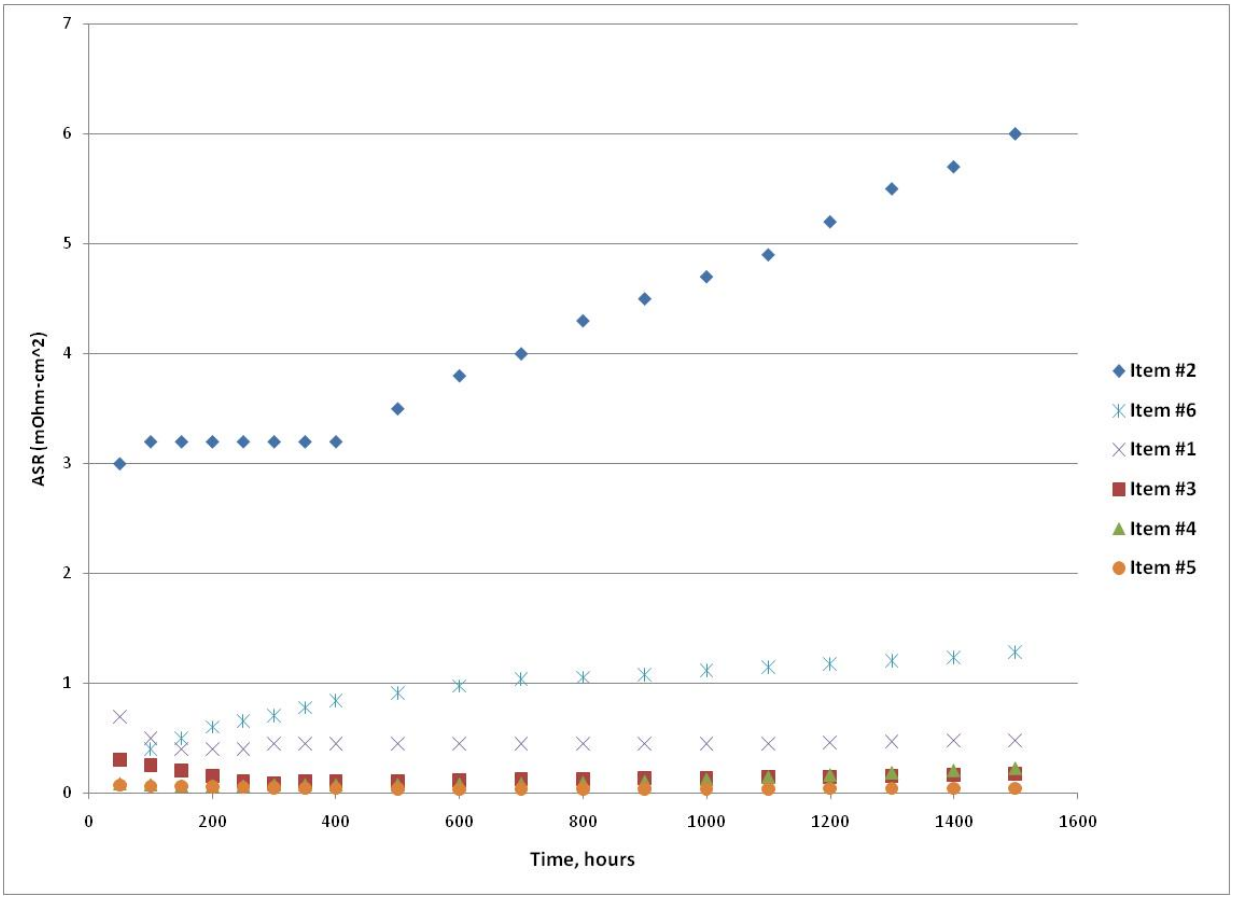

Figure 21. ASR data for LAFAD coatings presented in **Table 3**.

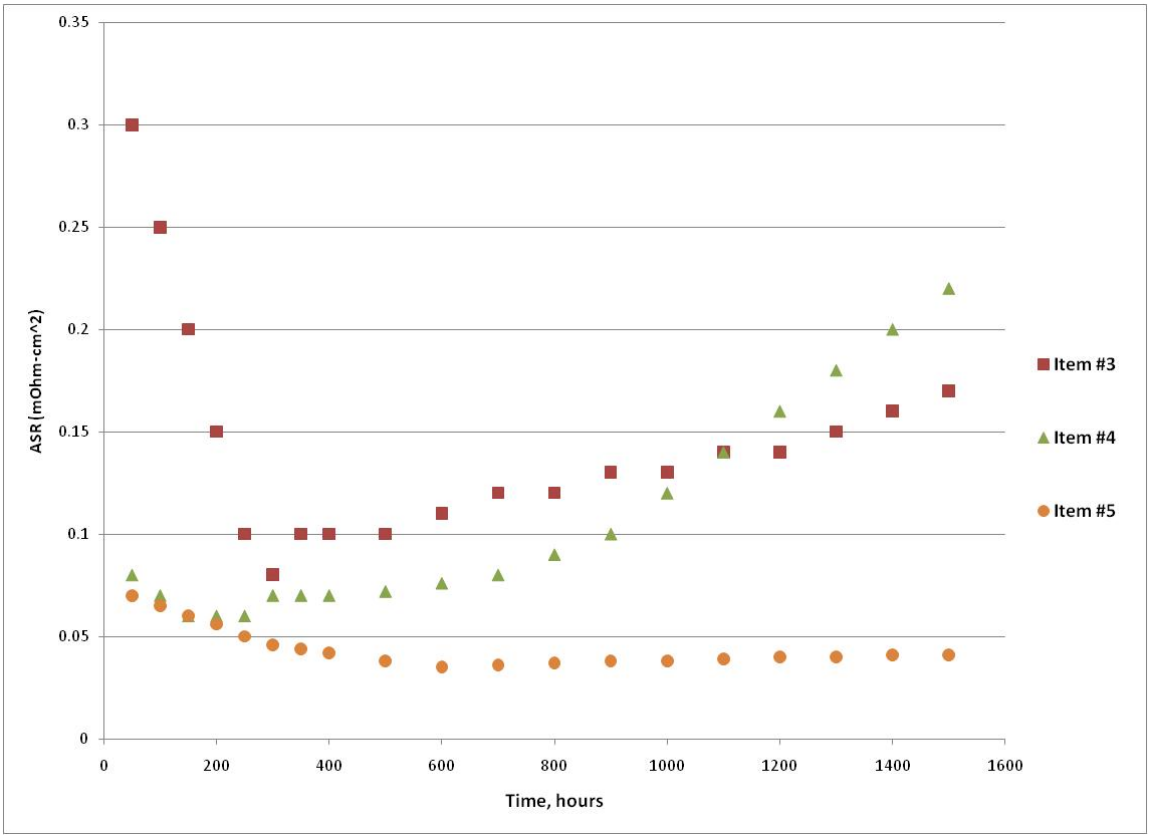

Figure 22. ASR data for LAFAD coatings in Table 3 (lower ASR scale).

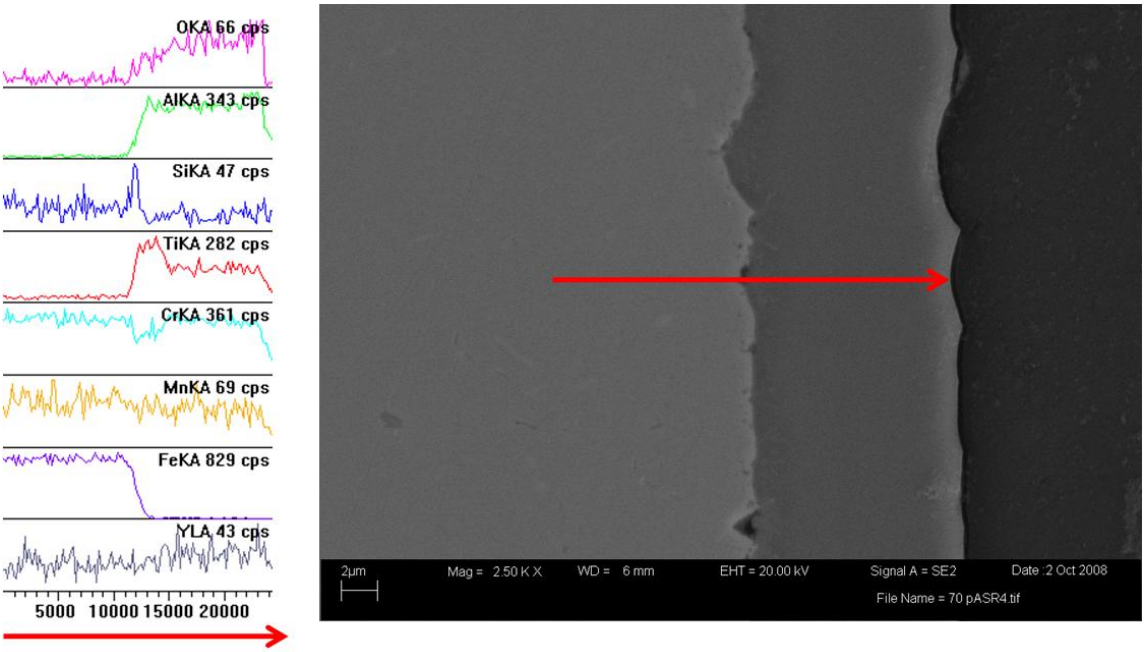

Figure 23. SEM cross section with EDS linescan of LAFAD TiCrAlYO coating after 1500 hours in 800°C air.

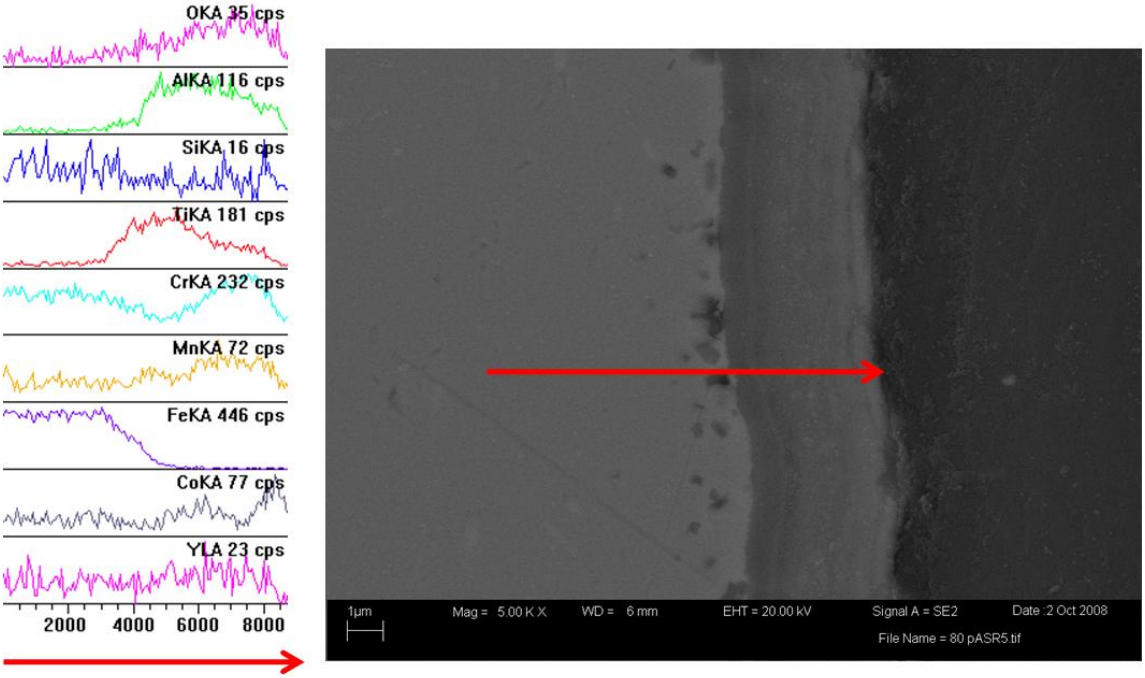

Figure 24. SEM cross section with EDS linescan of LAFAD CoTiCrAlYO coating after 1500 hours in 800°C air.

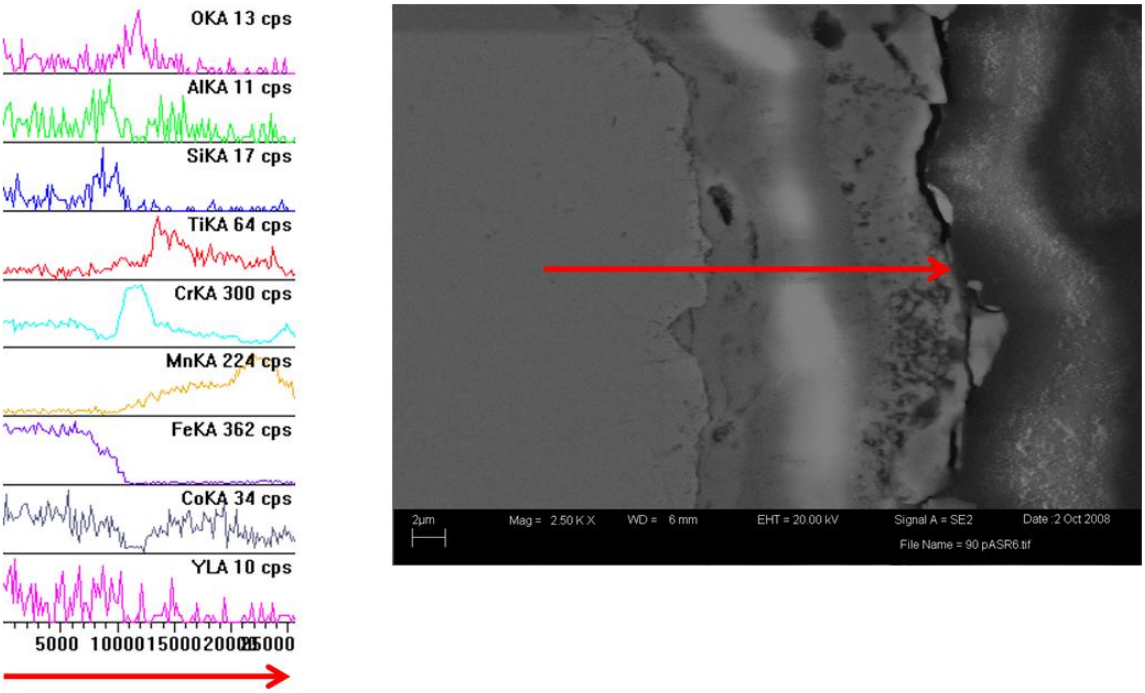

Figure 25. SEM cross section with EDS linescan of LAFAD CoMnTiCrAlYO coating after 1500 hours in 800°C air.

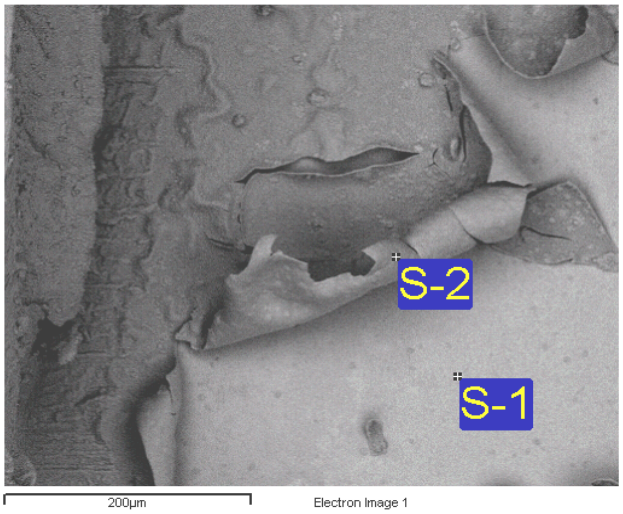

Figure 26. SEM surface image showing Phase I coating spallation following 1,000 hours in 800°C air (courtesy Versa Power Systems).

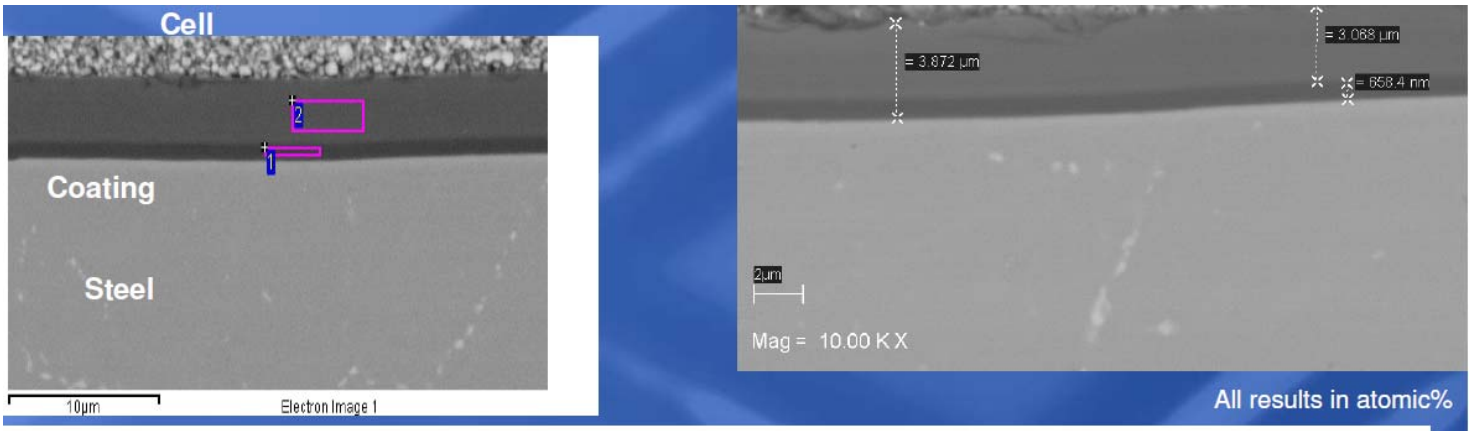

Spectrum	O	Al	Ti	Cr	Mn	Fe	Co	Y	Ag
1	50.58	23.07	4.22	13.15	0.75	6.03	1.19	0.59	0.41
2	56.08	20.31	3.59	13.73			5.17	0.56	0.57

Figure 27. SEM cross section of Phase II coating on SOFC(IC) following unsuccessful SOFC stack testing (courtesy Versa Power Systems).

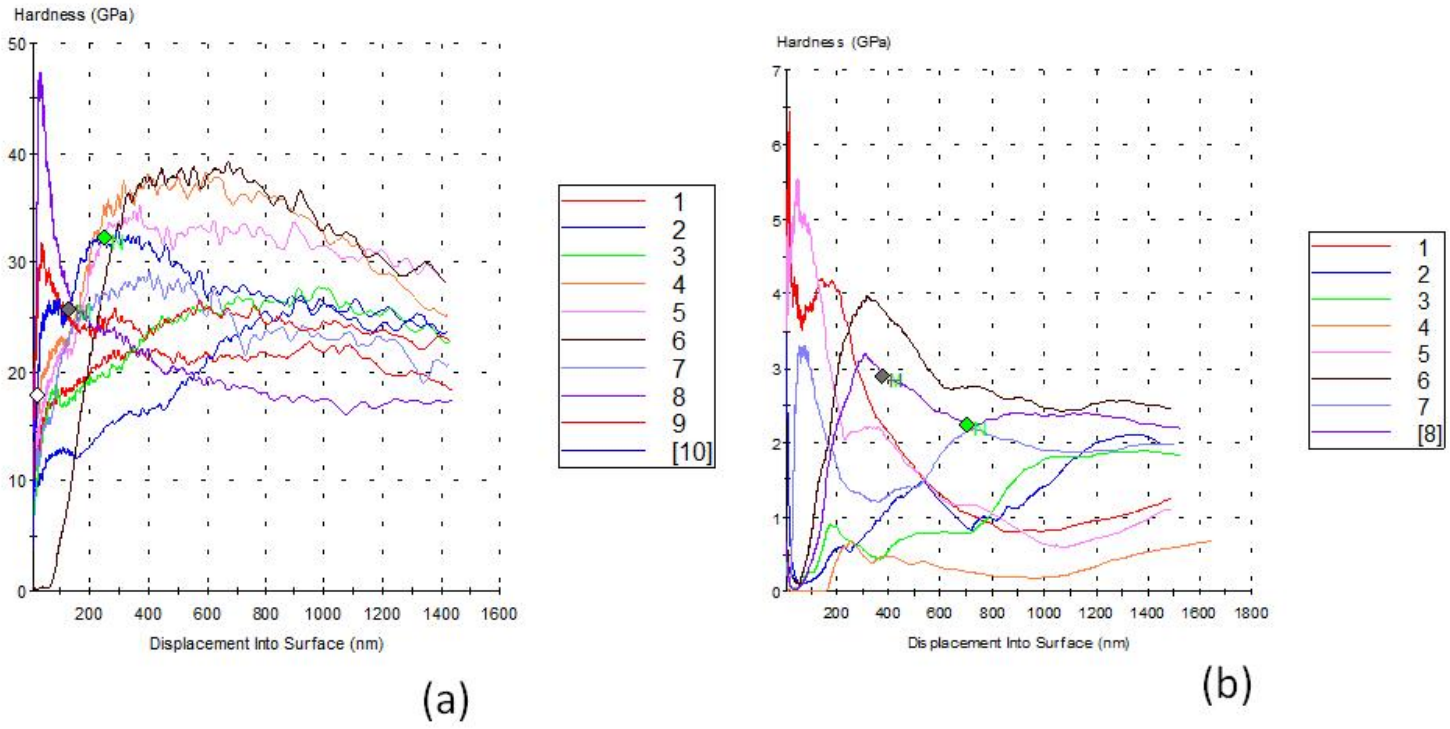

Figure 28. Nanoindentation plots for TiCrAlYO coating (**Table 3**, Item 2) (a) and CoMnTiCrAlYO coating (**Table 3**, Item 4) (b).

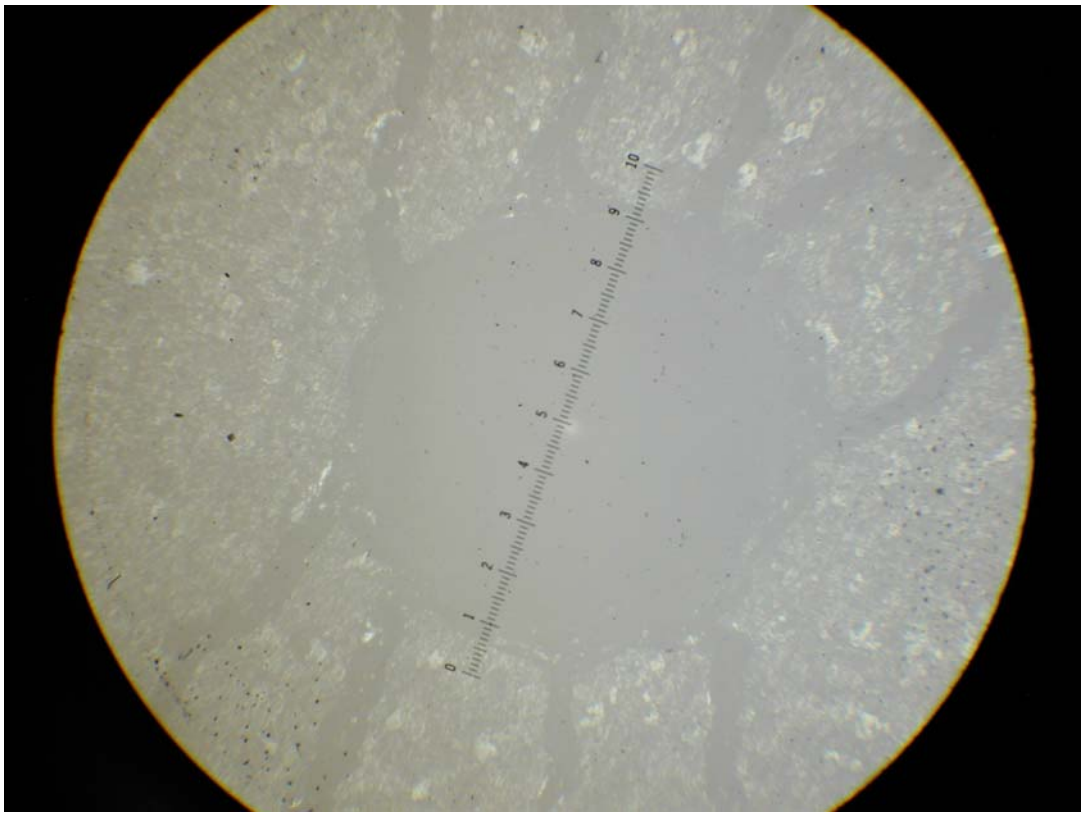

Figure 29. Optical micrograph of the Rockwell-C 145 kg indentation mark of TiCrAlYO 12 μm thick LAFAD coating on FSS substrate (**Table 3**, Item 2) after 1500 hours of exposure at 800°C in moisturized air.